Published September 7, 2012

Reviews and Analyses

N. K. Karadimitriou*
S. M. Hassanizadeh

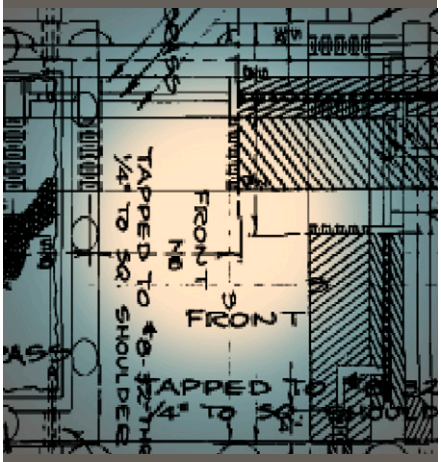

A Review of Micromodels and Their Use in Two-Phase Flow Studies

During the last 25 to 30 yr, micromodels have been increasingly used to study the behavior of fluids inside microstructures in various research areas. Studies have included chemical, biological, and physical applications. Micromodels have proven to be a valuable tool by enabling us to observe the flow of fluids and transport of solutes within the pore space. They have helped to increase our insight into flow and transport phenomena on both micro- and macro-scales. In this review, we have considered only the application of micromodels in the study of two-phase flow in porous media. Various methods exist for generating patterns used in micromodels. These include perfectly regular patterns, partially regular patterns, fractal patterns, and irregular patterns. Various fabrication methods and materials are used in making micromodels, each with its own advantages and disadvantages. The major fabrication methods include: Hele–Shaw; glass beads; optical lithography; wet, dry, and laser or plasma etching; stereo lithography, and soft lithography. The distribution of phases in micromodels can be visualized using (confocal) microscopes, digital cameras, or their combination. Micromodels have been applied to the study of two-phase displacement processes, measurements of fluid–fluid interfacial area and phase saturation, measurements of relative permeability, and the study of enhanced oil recovery.

Abbreviations: CCD, charge coupled device; PDMS, polydimethylsiloxane; PMMA, polymethylmethacrylate; UV, ultraviolet.

In this article, methods for generating networks of pores are described, as well as the means for manufacturing a micro-model. Various visualization setups are presented along with their advantages and limitations. The major applications of micro-models in two-phase flow, along with the necessary experimental parameters are also presented.

N.K. Karadimitriou and S.M. Hassanizadeh, Dep. of Geosciences, Univ. of Utrecht, Budapestlaan 4, 3584 CD, Utrecht, the Netherlands; S.M. Hassanizadeh, also Soil and Groundwater Systems Division, Deltares, Utrecht, the Netherlands. *Corresponding author (nikos@geo.uu.nl).

Vadose Zone J.
doi:10.2136/vzj2011.0072
Received 27 June 2011.

Micromodels are commonly used to investigate and visualize small-scale physical, chemical, and biological processes. One of the earliest micromodels was developed and used by Chatenever and Calhoun (1952) for investigating microscale mechanisms of fluid behavior in porous media. Since then, micromodels have been used to study many processes and applications involving two-phase flow. Examples include the capillary fingering effect, the percolation dimension (van der Marck and Glas, 1997), the fractal dimension (Lenormand and Zarcone, 1985a, 1985b; Lenormand, 1989a, 1989b; Lenormand et al., 1988), fluid flow through a nanometer-scale channel (Cheng and Giordano, 2002), and the labyrinth patterns in confined granular–fluid systems (Sandnes et al., 2007).

Strictly speaking, no clear definition of a micromodel in terms of two-phase flow in porous media has been articulated. A micromodel is an idealized, usually two-dimensional representation of a porous medium—a network of connected pores, measuring in the (tens of) microns, through which fluids flow and solutes spread. Moreover, visual observation of the flow of fluids and the movement of colloids or solutes should be possible in a micromodel. Accordingly, a micromodel is typically made of a transparent material that enables visual observation, such as glass or quartz, but it could also be polymeric. The requirement of small pores (<1 mm) is essential for two-phase flow studies because the capillary effects will be otherwise irrelevant. The overall size of a micromodel is typically on the centimeter scale. There must also be an inlet and an outlet area for the introduction and removal of the wetting and nonwetting phases. In summary, a micromodel, as defined here, is an artificial representation of a porous medium made of a transparent material. This fluidic device bears a flow network, with features on the microscale, and an overall size of up to a few centimeters.

Most micromodels have been considered as two-dimensional porous media; however, examples of three-dimensional micromodels can be found in the works of Montemagno and Gray (1995) and Avraam and Payatakes (1999). The difference between two-dimensional and three-dimensional micromodels relates to the limitations of the visualization setup. In principle, optical methods cannot be used for visualization throughout the depth of the model.

We present an overview of micromodels used in studying two-phase flow and transport in porous media and describe methods for generating the network of pores, as well as the

means of manufacturing a micromodel. Our focus then shifts to the various visualization setups used, and we investigate the application of micromodels in the field of two-phase flow in porous media.

The Micromodel Geometry

The early micromodels (Chatenever and Calhoun, 1952; Nuss and Whiting, 1947) had a simple and regular geometry. Later, micromodels were constructed with a more complicated geometry. Since the 1980s, the flow pattern of micromodels has been computer generated. We have generally classified micromodels based on the geometry and topology of the porous medium. Four main categories are identified and described below.

Perfectly Regular Models

In perfectly regular models, all pores have the same geometry—for instance, a square or rectangular cross-section throughout the entire domain. The pore depth and width and the distance between pores are constant throughout the whole network. Of course, some small variations may exist resulting from the manufacturing process. Examples of perfectly regular micromodels are those by Corapcioglu et al. (1997) used to visualize and quantify solute transport in porous media (see Fig. 1) and by Chen and Wilkinson (1985) used to examine viscous fingering.

Partially Regular Models

In partially regular micromodels, pore bodies and pore throats form a regular lattice and have the same cross-sectional shape; however, the pores' dimensions are variable. Pore sizes are chosen from a statistical distribution and may be correlated or uncorrelated. This pore size distribution determines the permeability of the network, as demonstrated by Tsakiroglou and Avraam (2002) (Fig. 2), Sbragaglia et al. (2007), and Chen and Wilkinson (1985).

Fractal Patterns

In some micromodels developed during the last few decades, the representation of the porous medium is based on fractals. The fractal patterns can be spatially correlated or not. A fractal micromodel may appear to have a completely irregular pattern, but actually it does not. Examples of such fractal patterns in natural rocks or flow networks in micromodels can be found in the works of Cheng et al. (2004), shown in Fig. 3, Nolte and Pyrak-Nolte (1991), Nolte et al. (1989), and Pyrak-Nolte et al. (1988). Flow networks that are generated in this way follow the rules of percolation theory. For flow to occur, its porosity has to be at least 50% for a correlated network and 60% for an uncorrelated network. If the porosity is lower than these limits, there is no connected path across the micromodel.

Irregular Patterns

For this category of networks, the main feature of the pattern and its geometry is a lack of spatial correlation. Pores are randomly placed in the network while their sizes are chosen from a single statistical distribution (see Sandnes et al., 2007; Fig. 4). The use of

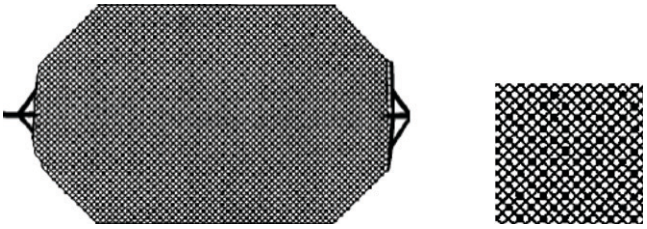

Fig. 1. Example of a micromodel with a perfectly regular pattern (left) and a magnified part of the micromodel (right) (Corapcioglu et al., 1997).

Fig. 2. Image of micromodel with a partially regular pattern (Tsakiroglou and Avraam, 2002).

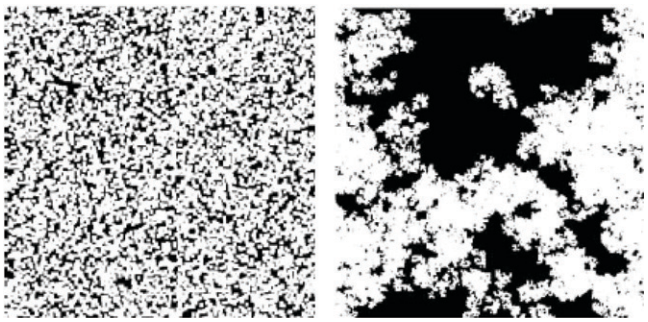

Fig. 3. Examples of micromodels with fractal patterns: spatially uncorrelated (left) and correlated (right) (Cheng et al., 2004).

Delaunay triangulation for generating the pattern can reproduce patterns that have properties that correspond well to real porous media, as shown by Heiba et al. (1992) and Blunt and King (1991). Delaunay triangulation requires that the connections between network nodes not intersect and that the triangular pattern of connections be as equilateral as possible.

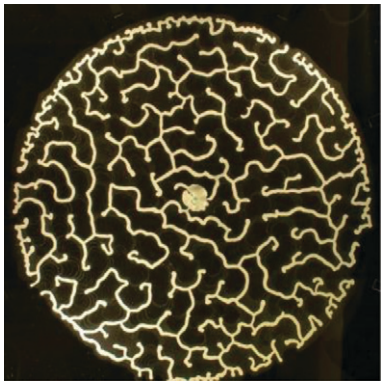

Fig. 4. Example of an irregular pattern micromodel (Sandnes et al., 2007).

Fabrication of Micromodels

Here we investigate the various techniques used in the fabrication of a micromodel. As mentioned above, the material that can be used to make a micromodel should be transparent. In this way, direct optical visualization of the flow and the distribution of fluids in the flow network is possible. Such materials are glass, quartz, polymethylmethacrylate (PMMA), and polydimethylsiloxane (PDMS). Another material that can be used is silicon. Below, we briefly describe the features and potential limitations of each material. The fabrication procedure needs to be accurate and efficient. New fabrication techniques have been introduced as micromodels have been increasingly used to study the behavior of fluids on a very small scale. For the sake of brevity, not all methods of fabrication are reported here but only those that are widely used.

Hele–Shaw and Glass-Bead Models

Chuoke et al. (1959) conducted one of the first studies of two-phase flow with a Hele–Shaw micromodel. Their work presented theoretical and experimental evidence for the existence of macroscopic instabilities in the displacement of a fluid by another immiscible fluid through a uniform porous medium. Hele–Shaw models are very simple in principle. They are made of two parallel transparent plates, with the flow taking place in the gap between them. The flow between two parallel plates is mathematically analogous to the flow through pores. This model is called a glass-bead model when glass or quartz beads or spheres are inserted between the two plates. The very first micromodel made by Alfred Chatenever and John C. Calhoun in 1952 at the University of Oklahoma is an example of a glass-bead model.

The micromodel of Chatenever and Calhoun (1952) consisted of an observation cell, as they called it, which was a single layer of glass spheres sandwiched between two flat plates. They found that using two or more layers made it difficult, given the available means of visualization, to distinguish one phase from another. The observation of flow phenomena was extremely complicated. They used different flow cells, one of which is shown in Fig. 5.

This micromodel was comprised of a Lucite base, a compression cover, an observation window, and a gasket. A glass plate was

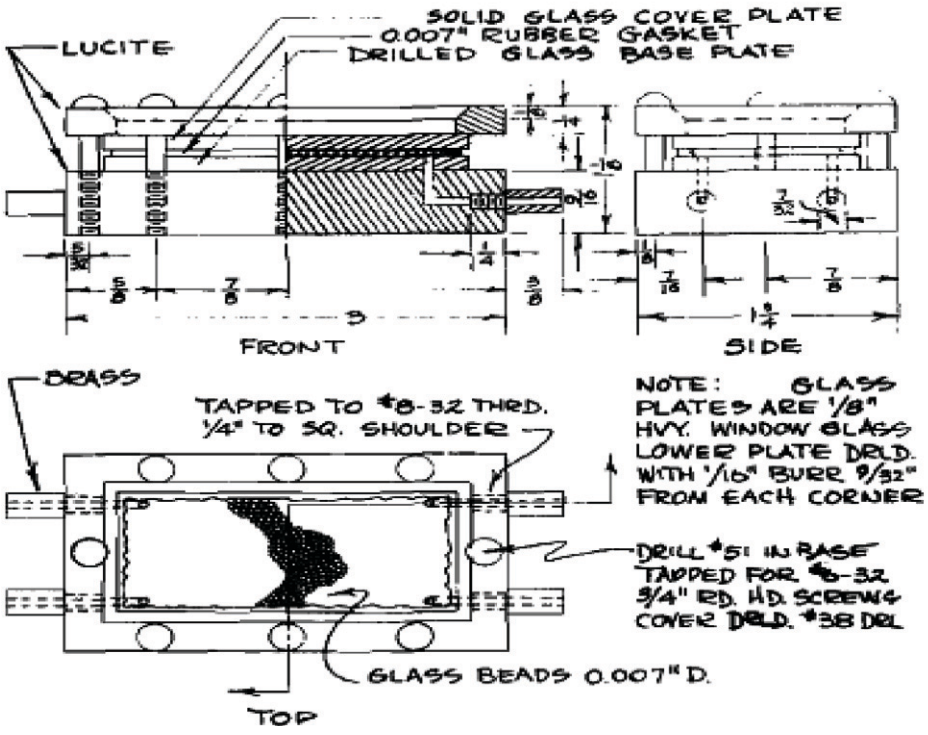

Fig. 5. Sketch of Type C cell by Chatenever and Calhoun (1952). All dimensions are in inches.

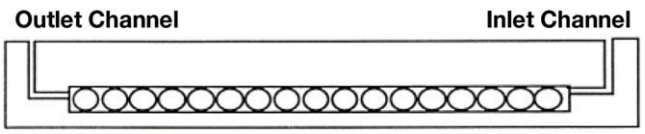

Fig. 6. Side view of a glass-bead micromodel (Corapcioglu and Fedirchuk, 1999).

molded into the Lucite base in a press to make an all-glass matrix composed of a glass top, glass spheres, and a glass base. The observation window was, in fact, the top cover of the cell. The spheres that were packed inside the cell formed a single-layered, rhombic, pore network pattern.

In Hele–Shaw and glass-bead micromodels, fluids are introduced into the model through a hole in the center of one plate (Sandnes et al., 2007) or at the ends of the parallel plates (Corapcioglu et al., 1997; Corapcioglu and Fedirchuk, 1999; Tóth et al., 2007; Lovoll et al., 2005, 2010; Tallakstad et al., 2009). Figure 6 shows the side view of a glass-bead micromodel of Corapcioglu and Fedirchuk (1999).

In principle, Hele–Shaw and glass-bead micromodels are easy to make. The use of optical microscopy poses a problem, however. The three-dimensional nature of the model makes it difficult, or sometimes impossible, to visualize the distribution of fluids under the level of the largest bead diameter. As such, much information cannot be recorded when optical means are used.

Optical Lithography

Developed during the last few decades, optical lithography (also called photo-lithography) has been used when a specific flow network has already been designed with preferred parameters, like mean pore size, number of pores, geometry of pores, etc., and its features are very small in size. Such models cannot be created from the combination of materials, as done in Hele–Shaw or glass-bead models. It can be used to make models that carry any flow network and has a wide application for irregular or fractal patterns. Optical lithography models are also relatively inexpensive to produce.

The principles of optical lithography were introduced in the early 1980s (Thompson et al., 1983, 1994). This method has been described in detail in the literature (see, e.g., Cheng et al., 2004; Giordano and Cheng, 2001). First, the desired pattern for the micromodel is produced digitally, based on a statistical distribution, with or without a spatial correlation for the pores. The desired flow network is then printed on a transparent material. The transparent material with the network printed on it is called a *mask*. There are two ways of using the mask. For relatively small networks, the network printed on the mask is the magnified image of the desired network. For large or deep networks, the network printed on the mask has the exact dimensions as the desired network. Usually for deep networks, the negative of the network is printed on the mask. In this case, a Cu-covered glass plate is used as a mask. The network is printed by removing the Cu layer from the mask. When the depth of the flow network is relatively low, the mask is a normal transparency and the network is printed as it is on the mask.

Optical lithography consists of the following general steps: (i) photoresist application on a glass substrate; (ii) soft bake; (iii) mask aligner setup; (iv) exposure; (v) development; and (vi) hard bake. The network is commonly formed in a polymeric material called *photoresist*. The glass substrate has to be made perfectly clean. After that, a thin layer of photoresist, usually SU-8, is applied to it and the substrate is spun. The type of photoresist and the duration of spinning determine the final thickness of the photoresist layer, which is, in practice, the final depth of the network. Then the substrate is soft baked to harden the photoresist.

The creation of the network on this layer of photoresist is the second step of the procedure. The mask is projected on the photoresist using ultraviolet (UV) light in a mask aligner. If the network has very small features, a transparency that carries a magnified image of the network can be used. This transparency is projected on the photoresist through an objective lens to bring the image back to the original size. In this way, the resolution of the projected image is improved. The area of the photoresist that is exposed to UV light reacts with developing agents. Next, the exposed area of the photoresist is washed away and what is left forms the flow network. When the network is deep, negative projection is used. In that case, the developed area is that which was not exposed to the UV light. The choice of development depends on the depth of the network and the type of photoresist that has been used.

The inlet and outlet areas are developed in the same way. For this, there is no need for a magnified mask and projection because the dimensions of these areas are large enough and details do not matter. The mask has the actual dimensions of these areas. Inlet and outlet areas should be strengthened to withstand the pressure imposed during the experiments. For this reason, pillars made of photoresist are added within inlet and outlet areas. Their dimensions are on the order of hundreds of micrometers. An example of a micromodel constructed following the optical lithography method is the one by Cheng and Giordano (2002) shown in Fig. 7.

A second glass plate is used as a covering plate to complete the fabrication of the micromodel. Two holes are drilled on this glass plate for the inlet and outlet of the model. The micromodel is sealed with a thin layer of photoresist on the upper glass plate. This layer acts like a glue and bonds the glass plate to the photoresist with the application of mechanical pressure. This layer also ensures that the micromodel pore walls are made of one material—namely, the photoresist only—avoiding mixed wettability in the model.

The optical lithography method is relatively inexpensive and easy to implement. These two characteristics make it quite attractive.

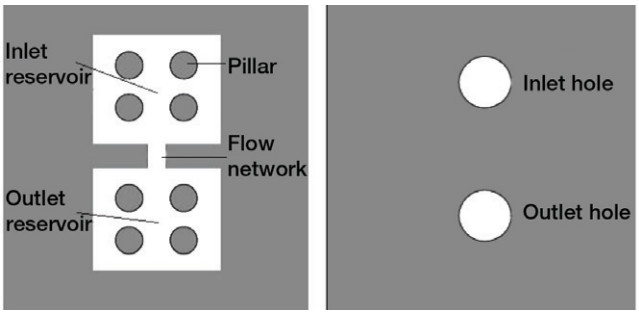

Fig. 7. Bottom and upper plates (left and right drawings, respectively) of micromodels constructed by Cheng and Giordano (2002).

Problems arise, however, in making and using this kind of micromodel. Significant difficulty in sealing the model can occur when some features of the flow network are very small. This happens because there is not enough surface for the bonding between the thin layer of photoresist that is used as glue and the photoresist from the flow network that is in a solid state.

Another major problem emerges from the photosensitive nature of photoresist. Even after baking, exposure to light with a wavelength close to the violet or UV spectrum causes the photoresist to produce N_2. The N_2 bubbles, also called *pockets*, grow in size, breaking the solid photoresist and gradually destroying the network. We reproduced this effect in the laboratory and the results are shown in Fig. 8. On the left, a photoresist micromodel filled with water can be seen on the first day of its use, and on the right, the same micromodel is shown after 3 d of exposure to light. The model has been significantly damaged by the production of N_2. One solution to this problem is to replace all lights in the laboratory where a photoresist micromodel is being used with lights that have a spectral emission >550 nm. This will ensure that there is no interaction between the photoresist and the light. Also, the wavelength of observation lighting should be away from the violet region. Another solution is to use filters that cut off all wavelengths <550 nm. In practice, both solutions are effective but both require extra expense. In particular, the high-quality optical filters necessary to eliminate the undesired wavelengths can be very expensive.

Etching Method

The first etched micromodel was constructed by Mattax and Kyte in 1961 (Fig. 9). The fabrication technique is based on chemical reactions and the interaction of laser and plasma radiation with glass, silicon, or polymer (Zhang et al., 2010, 2011a, 2011b; Baouab et al., 2007; Gutiérrez et al., 2008; Soudmand-asli et al., 2007; Weidman and Joshi, 1993; Jeong and Corapcioglu, 2003, 2005; Baumann et al., 2002; Lanning and Ford, 2002; McKellar and Wardlaw, 1982). First, the desired pattern for the micromodel is produced with one of the methods mentioned above. The mask is prepared in one of the ways explained for optical lithography, depending on the size and the depth of the desired network; the mask can be made to be the positive or the negative image of the network.

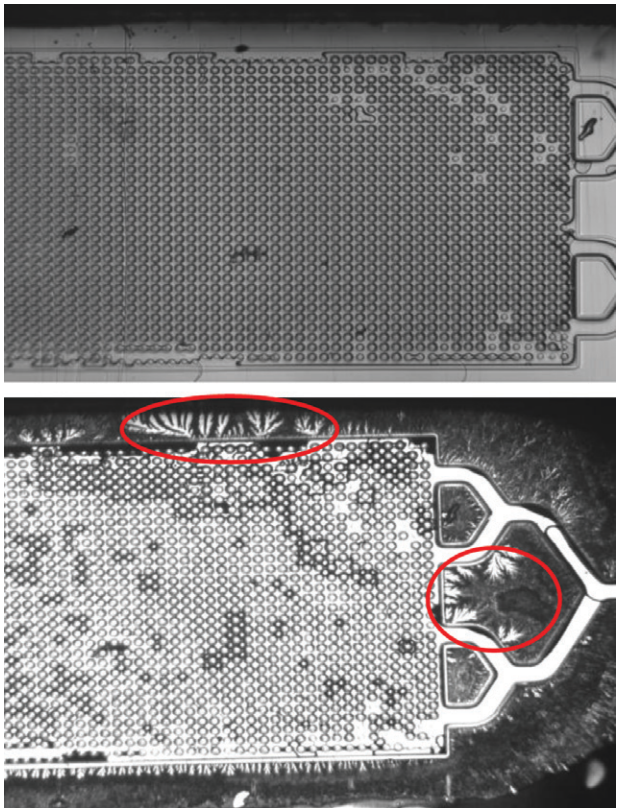

Fig. 8. A photo-resist micromodel on the first day of its use (left) and the same micromodel after 3 d (right). The fractures in the photo-resist can be seen clearly (red outlines).

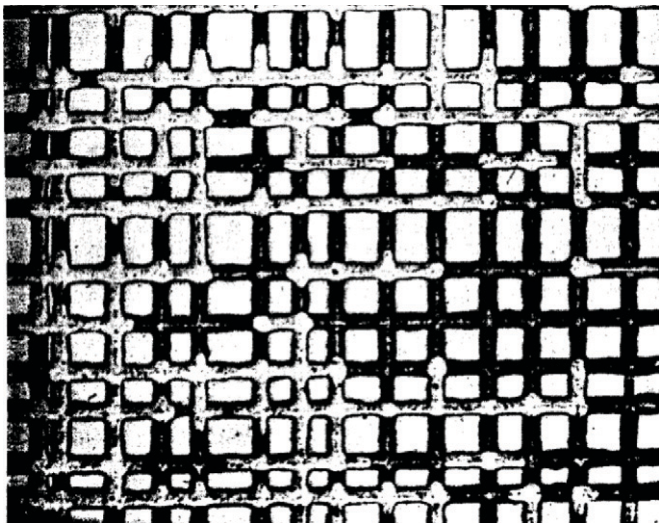

Fig. 9. Capillary network in a portion of an etched micromodel (Mattax and Kyte, 1961).Oil Gas Journal

The desired pattern is projected onto a glass substrate that has already been covered with a layer of photoresist, as in photo-lithography, but in this case the network is formed in the glass substrate and not in the photoresist. The resolution of the mask strongly affects the outcome of the etching process. The thickness of the photoresist will determine the depth of the desired flow network after the development of the network with the use of solvents. After the pattern is developed and exposed, the network is created using an etching method. Currently, there are two etching methods.

Chemical or Wet Etching

In chemical or wet etching, acids are used as etchants to etch the glass or silicon surface (Wegner and Christie, 1983; Johnston, 1962; Sagar and Castanier, 1998; Coskuner, 1997; Avraam et al., 1994; Sirivithayapakorn and Keller, 2003; Lago et al., 2002; McKellar and Wardlaw, 1982; Hornbrook et al., 1991; Upadhyaya, 2001; Jeong et al., 2000; Wan et al., 1996). The area covered by photoresist remains unaffected by the acid. The depth of penetration depends on the etching rate of the acid (i.e., the penetration length with time) and the time of exposure to the etchant. Alternatively, Cu can be used instead of the photoresist in lithography process. The Cu then can be removed with the use of chemicals.

The wet etching process in an acidic bath, apart from the photo-lithographic step, may be broken down into three basic steps: (i) diffusion of the etchant to the surface for removal; (ii) reaction between the etchant and the material being removed; and (iii) diffusion of the reaction byproducts from the reacted surface. Wet etching is a very popular way of making micromodels; however, this method has some limitations

One shortcoming is that the pore walls are sloped rather than vertical. Also, there is a curvature at the bottom of pores. This happens because liquid acids are isotropic and thus erode glass in all directions. Figure 10 (from Iliescu et al., 2008) shows in black the microchannels formed by the wet-etching technique on a glass substrate. The curvature at the bottom of the walls and the optical setup used to take the pictures create refraction, leaving no light to reach the camera's sensor. This effect hinders studying two-phase flow, especially if the optical visualization of fluids and their configuration in the network are important. One remedy would be to diffuse the illumination and increase the intensity of the light. Another effective solution is to use front-light illumination instead of back-light illumination. In this case, a strong contrast between the sample and the background is needed.

Plasma or Laser Etching

Electromagnetic radiation provides another way to etch glass or other transparent polymeric materials like PMMA or silicon. The radiation can be supplied from a laser source or from a beam of ions. The latter method is called *ion milling* when using a noble-gas plasma (Durandet et al., 1990; Kolari et al., 2008). The most popular noble gas for this purpose is Ar^+. Using an ion gun, ions

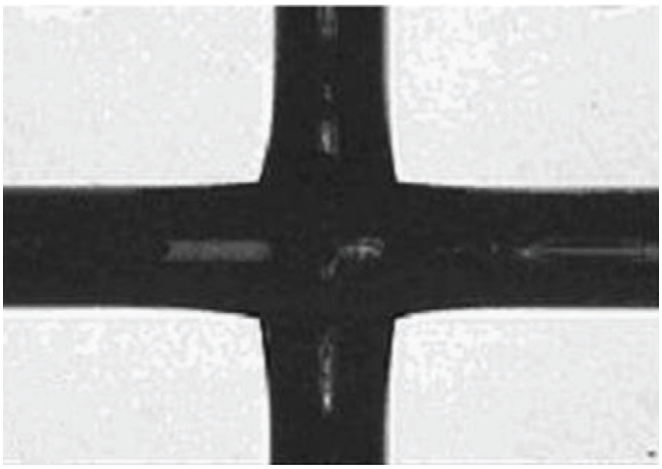

Fig. 10. Optical image showing the intersection of two microchannels (approximately 150 μm in depth) etched in glass for 20 min in 49% HF solution using an amorphous Si mask with a value of 100 MPa (from Iliescu et al., 2008). The curved walls produce diffraction and the optical result is black.

bombard the uncovered area and, by transfer of momentum, begin removing atoms from the glass surface.

The reactive-ion etching process, apart from the photo-lithographic step, can be broken down into the following steps: (i) etchant species (radicals or ions) generation; (ii) reaction or momentum transfer with the surface; (iii) byproduct desorption; and (iv) diffusion of the byproduct to bulk gas.

Instead of ion milling, excimer (Basov et al., 1970) laser can be used to create the pattern on the glass substrate (Arnold et al., 1995). The technique is called LIGA (Lithographie, Galvanoformung, Abformung) and was introduced by Ehrfeld et al. (1987, 1994, 1996). The network pattern is directly formed on the substrate and the whole procedure is computer controlled.

Both procedures are very anisotropic, which means that the sloping effect at the walls is diminished; however, control of the whole procedure is not easy. This procedure is usually reserved for very narrow and shallow channels. After the pattern has been created on the glass substrate, the inlet and outlet reservoirs are produced with wet-etching techniques. A second glass plate, in which two holes are drilled for the input and output, is used to cover the micromodel.

The sealing of the micromodel can be done in two ways, both of which are common for both wet- and dry-etched micromodels. One way is the use of a muffle furnace or high-temperature oven (Avraam et al., 1994). This method is used mostly for micromodels that are multilayered. The other method involves placing a thin layer of polymer (a few nanometers thick) between the two glass plates and baking in a UV oven (Tsakiroglou and Avraam, 2002). Heating the model and simultaneously applying a light pressure

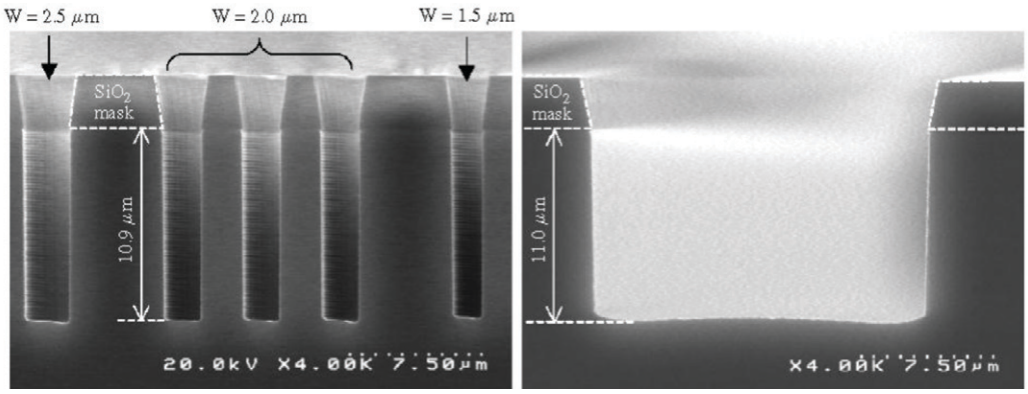

Fig. 11. Mask openings and the channels produced with the dry etching method; channel widths are 1.5 to 2.5 μm (left) and 20 μm (right) (Ohara et al., 2010).

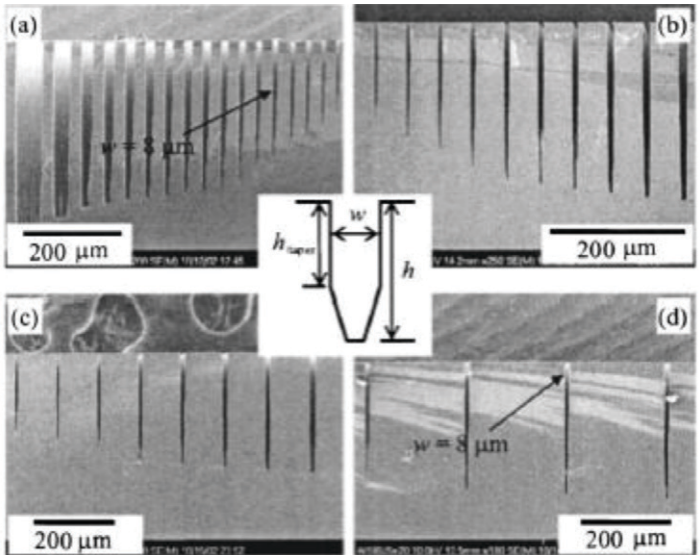

Fig. 12. Scanning electron micrograph images of silicon trenches etched by the inductively coupled plasma–deep reductive-ion etching process for 3 h (Yeom et al., 2005). These are from four different initial pattern area densities: (a) 80% microloading (explained in Hedlund et al., 1994) with 25-μm line spacing, (b) 50% microloading with 50-μm line spacing, (c) 30% microloading with 100-μm line spacing, and (d) 10% microloading with 200-μm line spacing.

will have the desired effect for glass–glass bonding. Silicon and glass bonding can be achieved by gentle heating (~400°C) while applying an electric field across the silicon–glass sandwich to ensure good contact via the associated electrostatic force. This method is known as *field-assisted* or *anodic bonding* (Giordano and Cheng, 2001). Anodic bonding will work only for moderate operating pressures of a few hundred kilopascals within the micromodel. Other methods should be used if larger pressure must be applied (Hollman and Little, 1981; Little, 1982).

Dry-etching methods produce nearly vertical walls (82–90°). The deep reactive-ion etching (DRIE) method, which is a plasma-etching method, also produces nearly vertical walls (88–90°) with a very low surface roughness. The DRIE method can give good results for ratios between the depth and the width of an etched channel even greater than 20:1. There is still a maximum achievable aspect ratio between the depth and the width of the channel, however, that depends on the material, the beam profile, etc. (Blauw et al., 2001; Yeom et al., 2003; Willingham et al., 2008).

Figure 11 (Ohara et al., 2010) shows that where the ratio between the depth and the width of the channels is from 6.6:1 to 1:2, the walls are vertical and the roughness of the bottom of the channels is low.

When the channels are deep and very narrow, it becomes difficult to get vertical walls and keep the roughness at the bottom of the channel low. Figure 12 (Yeom et al., 2005) shows that as the ratio of the depth to the width of the channels becomes larger, the quality of the channels becomes lower. The surface roughness increases and we don't get a rectangular shape at the bottom. Although such

channels are not common to two-phase flow in porous media, they are presented here as an extreme example of reactive-ion etching.

The reactive-ion etching method is a complicated and difficult procedure and many things can go wrong. Etching itself is a subject of ongoing research. Given our current knowledge, however, etching remains one of the best ways to make good-quality micromodels. Especially when optical microscopy with back-light illumination is used, etching is perhaps the best alternative. In particular, the stability of glass with respect to its chemical and physical properties is highly appreciated.

Stereo Lithography

Stereo lithography is a computer-based manufacturing process that was developed by Hull (1986). As described by Melchels et al. (2010), it is a solid, free-form fabrication technique. Stereo lithography is an additive fabrication process that allows the fabrication of parts using a computer-aided design (CAD) file. The manufacturing of three-dimensional objects by stereo lithography is based on the spatially controlled solidification of a liquid resin by photo-polymerization. The setup consists of a computer-controlled laser beam or digital light projector, a computer-driven building stage with a platform, and a resin reservoir. The platform is initially placed just below the resin surface, according to the desired depth of the resin layer. The computer guides the laser beam to follow a path and illuminate a desired pattern on the resin surface. As a result of this, the resin in the pattern is solidified to a prespecified depth, causing it to adhere to the support platform. After photo-polymerization of the first layer, the platform is lowered incrementally, allowing the built layer to be recoated with liquid resin. Each time, the pattern is cured (i.e., solidified) to form another layer. As the depth of curing is slightly larger than the platform step height, good adherence to the first layer is ensured (i.e., unreacted functional groups on the solidified structure in the first layer polymerize with the illuminated resin in the second layer). These steps (i.e., the movement of the platform and the curing of a pattern in a layer of resin) are repeated until a solid, three-dimensional object of the desired height is constructed. After draining and washing off excess resin, the desired structure is obtained. In this structure, the conversion of reactive groups is usually incomplete, and post-curing with (stroboscopic) UV light is often used to improve the mechanical properties of the structures. In Fig. 13, a schematic presentation of the process is presented.

To summarize, the stereo lithography fabrication method consists of the following steps: (i) laser beam formation of the desired pattern on the resin surface; (ii) photo-polymerization; (iii) incremental lowering of the platform; (iv) following of the previous steps; and (v) cleaning excess resin from the structure as soon as construction is finished.

Stereo lithography is an effective way to make micromodels when the dimensions of the structure are not very small (larger than

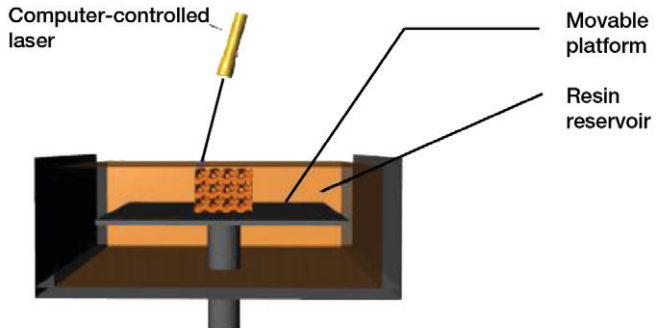

Fig. 13. Schematic presentation of a bottom-up stereo-lithography system with scanning laser (Melchels et al., 2010).

micrometers). Parts from a larger assembly (not micromodels but general structures) can be manufactured in 1 d and with great efficiency. The complexity of a flow network or a part of an assembly is not an issue. On the other hand, this procedure is quite expensive. Stereo-lithographic micromodels have been used in studying flow (Crandall et al., 2008, 2009; Stoner et al., 2005; de Zélicourt et al., 2005). They have been less popular, however, for very small dimensions (micrometer scale) because of the spatial resolution of the process.

Soft Lithography

Soft lithography refers to methods for making structures using "soft" materials like elastomeric stamps, molds, and photo-masks (Quake and Scherer, 2000; Rogers and Nuzzo, 2005; Wang et al., 2005, 2008; Shor et al., 2004). It is mostly reserved for creating very small, simple geometric structures on the micro- and nanometer scales (Hug et al., 2003; Huh et al., 2007; Park et al., 2009). Variations of the soft lithography method include micro-contact printing (μCP) (Xia and Whitesides, 1998; Fig. 14), replica molding (REM) (Senn et al., 2010), micro-transfer molding (μTM) (Xia and Whitesides, 1998), micro-molding in capillaries (MIMIC) (Kim et al., 1996), and solvent-assisted micro-molding (SAMIM) (King et al., 1997). These methods are particularly suitable for creating micrometer-scale structures, the scale of interest in two-phase flow, where soft lithography is most accurate.

One of the most widely used materials in soft lithography is PDMS, which is an elastomeric material. It is a liquid that is polymerized after mixing with a curing agent. The procedure for manufacturing a PDMS micromodel was explained in detail in Quake and Scherer (2000), Auset and Keller (2004), and Markov et al. (2010). Usually, it consists of the following steps: (i) the network of micromodel channels is created digitally and printed on a transparency, which is used as a mask in the next step; (ii) a silicon or glass wafer is spin-coated with photoresist (positive or negative depending on the desired depth) to create a patterned silicon or glass wafer (called a *master*) by using photo-lithography; (iii) the master wafer is put in a petri dish and a mixture of liquid PDMS and curing agent is prepared, which is then poured over the master wafer in the petri dish; (iv) the polymer is

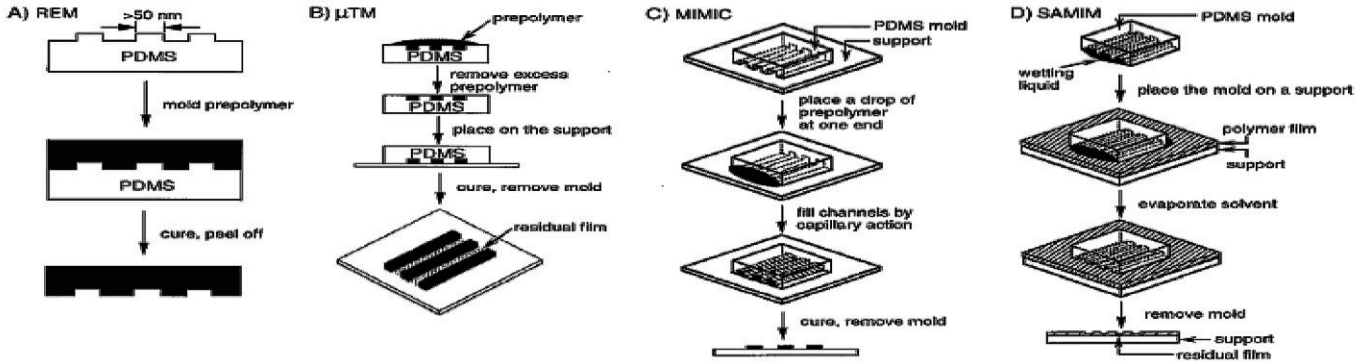

Fig. 14. Schematic illustration of procedures for (A) replica molding (REM), (B) microtransfer molding (μTM), (C) micromolding in capillaries (MIMIC), and (D) solvent-assisted micromolding (SAMIM) using polydimethylsiloxane (PDMS) (Xia and Whitesides, 1998).

Table 1. Micromodel fabrication methods along with their advantages and disadvantages.

Fabrication method	Advantages	Disadvantages	Major references
Hele–Shaw and glass beads	easy to make, choice of wetting properties, cheap to make, no mask needed	fixed or random network geometry cannot be used under dynamic conditions because the lower half of the model cannot be visualized	Corapcioglu et al. (1997), Corapcioglu and Fedirchuk (1999), Chatenever and Calhoun (1952)
Optical lithography	accurate, can reproduce any network pattern, cheap to make	not suitable for making elongated models due to the manufacturing procedure, fixed wetting properties, cannot be exposed to regular light, requires a clean room to manufacture, mask needed	Thompson et al. (1983, 1994), Cheng et al. (2004)
Wet etching	relatively easy, choice of wetting properties depending on the chosen material, can reproduce any network pattern	curvature on the walls makes back-light illumination impossible, limited ratio between pore width and depth, mask needed	Wegner and Christie (1983), Johnston (1962), Sagar and Castanier (1998)
Deep reactive ion etching, laser etching, ion etching	highly accurate, can reproduce any network pattern	limitation on the depth of the model, maximum ratio between width and depth, very expensive	Yeom et al. (2003), Ohara et al. (2010)
Stereo lithography	three-dimensional structures	low resolution, very expensive	Hull (1986), Melchels et al. (2010)
Soft lithography	highly accurate, easy to make, can reproduce any network pattern, cheap to make	needs treatment to fix wettability issues, needs clean room to prepare the silicon wafer	Xia and Whitesides (1998), Kim et al. (1996, 1997)

degassed under vacuum and then cured; (v) after curing, the polymer is peeled from the master; and (vi) the PDMS slab with the desired network is placed on a pre-cured thin slab of PDMS to close the network and exposed to ion plasma so that bonding can take place.

Soft lithography is widely used in two-phase flow studies. It is a method that produces detailed micromodels without severe production restrictions. One problem does arise, however. Because they are polymeric materials, their wetting properties may change with time. For instance, PDMS is initially hydrophobic, although not strongly. In the making of an all-PDMS micromodel, the two parts of the model are bonded with O_2 plasma. The treated PDMS becomes hydrophilic but the effect is not stable; it degrades with time and the PDMS eventually recovers its hydrophobicity. This effect starts almost immediately after exposure, and it continues for hours, or even days, until the material reaches its initial condition (Murakami et al., 1998; Fritz and Owen, 1995). Thus, if hydrophilic behavior is needed, the micromodel must be used directly after its plasma treatment.

An alternative treatment is to force the PDMS surface to have specific wetting properties and become purely hydrophobic. This can be done with the application of a mixture of silane with ethanol (Zhou et al., 2010).

Another consideration is that the phases involved in the experiments should not make the material swollen or deformed. Gervais et al. (2006) studied the flow-induced deformation of PDMS models and provided a dimensionless number as a simple means of assessing whether deformation should be considered. This dimensionless number depends on the pressure drop along the network, the network's height and width, as well as the entry pressure of the features of the network. Depending on the value of this dimensionless number, deformation can be considered as important or not.

In Table 1, the fabrication methods along with their main advantages and disadvantages and major references are presented.

Micromodel Materials

Glass and quartz are materials that are widely used in micromodels, especially in Hele–Shaw and glass-bead micromodels. It is relatively easy to find well-polished glass or quartz plates or glass beads with a given diameter at a high accuracy. While the construction of glass-bead micromodels is relatively easy, the creation of a flow network in glass or quartz plates is quite involved. If the flow network has to meet some stringent requirements, however, such as vertical walls, stable wettability properties, or mechanical and chemical stability, then glass or quartz is the material of choice. This creates some problems, given their physical properties.

Glass micromodels are relatively cheap to make using the chemical etching method. This cannot be done in a regular laboratory environment, however, because of the use of acids. This should be done in a well-controlled environment, like a clean room. When ion etching is used, it is impossible to make them in a regular laboratory. The whole procedure requires a specialized infrastructure, takes a lot of time, and is very expensive. Moreover, to date, there is an upper limit of about 20 to 30 μm on the maximum etched depth that can be reached with the channels still having a rectangular cross-section. Additionally, there is a high probability that the whole procedure can fail in the last step of manufacturing, which is sealing the model. This is especially difficult if the features of the flow network are very small, not providing enough surface for bonding. Finally, given the cost in time and money, very careful handling is required with glass micromodels because they can break easily.

On the other hand, glass micromodels are stiff and rigid, and if the depth of the flow network is kept small (up to 20 μm) the whole manufacturing procedure can be well controlled. This provides very high quality micromodels that are practically insensitive to room temperature changes, have very well-defined wetting properties, can withstand pressures up to a few hundred kilopascals, and hardly react with fluids that are commonly used in two-phase flow studies.

Soft materials, like PMMA and PDMS, are suitable for making inexpensive micromodels fast. Polymethylmethacrylate, which is harder than PDMS, is an acrylic thermoplastic material, which is a good substitute for glass. It is not as rigid and stiff as glass, thus it is easier to treat. It can be etched with laser radiation, with the use of ions, or chemically. Polydimethylsiloxane micromodels are very cheap to produce and can be made in a normal laboratory; however, a master wafer is needed on which the flow network is formed, which has to be prepared in a clean room. This wafer then can be used to prepare from 10 to 15 micromodels in a normal laboratory.

While soft materials have the advantage of being very cheap and relatively easy to make and do not require a special laboratory (as in the case of PDMS), there are some limiting issues. They react or absorb fluids and chemicals that are commonly used in two-phase flow studies. This results in a deformation (swelling) of the material, which changes the properties of the flow network. For PDMS, there are some well-known mixed wettability issues and property changes with time. Special treatment may help, but it is not always effective. These materials can deform under moderate pressures (less than 100 kPa), resulting in breaking the model in the case of PMMA or destroying the bonding in the case of PDMS.

Silicon micromodels can be made in the same way as glass ones. Because of the different physical properties of the materials, tuning parameters should be properly adjusted, but the processes remain the same. They have severe limitations, however, if they are to be used for two-phase flow studies. A major problem is that silicon is translucent and therefore a wholly silicone-made micromodel cannot be used for direct optical visualization. They are usually sealed with glass or another transparent material. This means that the fluids involved will experience the presence of two different materials, with two different wetting properties. This is usually not desirable in two-phase flow studies. On the other hand, silicon micromodels provide the same advantages as a glass micromodel.

Micromodel Visualization Methods

Basic Issues

Since their inception, a challenge in using micromodels has been the ability to monitor fluid configuration, fluid flow, and various features inside the micromodel. The choice of the visualization method is essential to the outcome of any experiment. In a two-phase flow experiment, the average saturation and specific interfacial area are two of the main variables of interest. The measurement of these variables is based on the study of pictures or videos. Given the dimensions of the pattern in a micromodel, the demands on resolution and color depth are quite strict. Moreover, in the case of dynamic experiments, where the fluid distributions need to be recorded as a function of time, a high image acquisition rate from the visualization setup is also required.

Chatenever and Calhoun (1952) used cine-photo-micrography in their experiment. The apparatus consisted of a microscope and its accessories (lenses, mounts, etc.), a 16-mm movie camera, a beam splitter, an arc illuminator, and an exposure meter. They obtained images of fluid distribution during an oil-flood experiment (Fig. 15).

The methods used to monitor two-phase flow, statically or dynamically, may be classified in four groups. These are methods making use of a microscope alone or along with a camera, the photo-luminescent volumetric method, and fluorescent microscopy.

A Microscope–Camera Visualization Setup

This monitoring setup is quite simple. The micromodel is put under the objective lens of a microscope. The camera is mounted on the ocular of the microscope (Rangel-German and Kovscek, 2006; Keller et al., 1997; Corapcioglu et al., 2009; Vayenas et al., 2002;

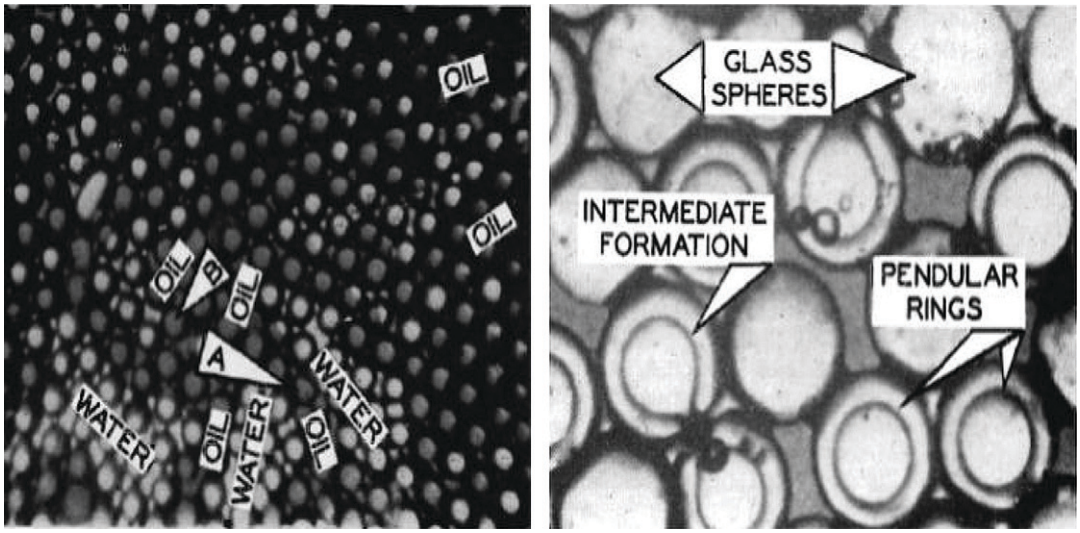

Fig. 15. Photomicrographs taken by Chatenever and Calhoun (1952) during an oil-flood experiment using uniform spheres with a 0.1778-mm (0.007-inch) radius: a portion of the channel flow structure established in an observation flow cell (left) and magnification of a part of the image showing the fluids configuration and the final pendular rings formed during the oil flood (right).

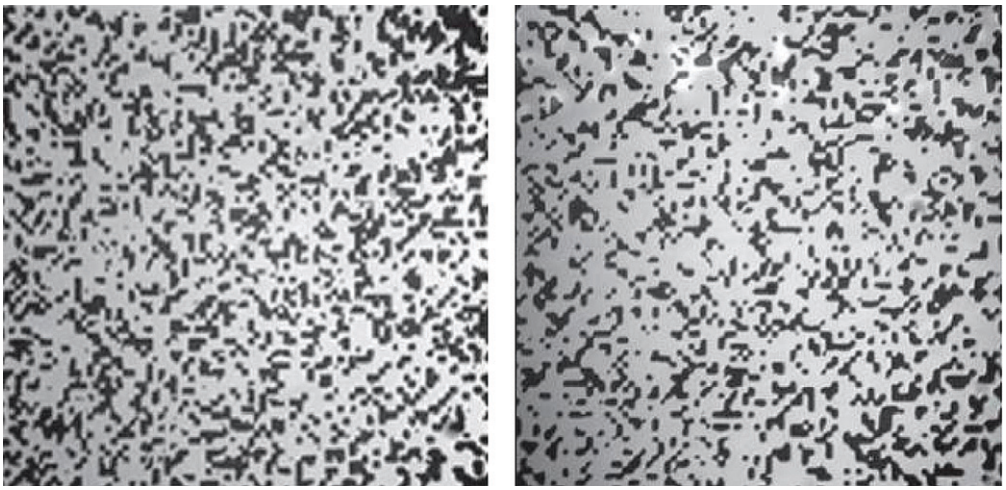

Fig. 16. Images taken from a micromodel's flow network taken with a Qimaging Retiga EX camera through an Olympus microscope from a pattern with an aperture of 2 μm (left) and with 1-μm aperture (right) (Pyrak-Nolte et al., 2008). The size of the domain is 600 by 600 μm.

Paulsen et al., 1998). The camera is connected to a computer to allow rapid data acquisition that can be stored in the computer. Images are processed and analyzed with appropriate software. From such an analysis, average saturation and specific interfacial area can be determined (Cheng, 2002; Pyrak-Nolte et al., 2008; Cheng et al., 2004; Chen et al., 2007). Figure 16 shows images obtained through this visualization method.

This technique is used when there is a need for a very high resolution—for example, when the smallest pore sizes are 1 to 2 μm or variables such as the interfacial area need to be determined. This technique is not applicable when the micromodel is elongated and dynamic effects are being studied. The reason is that the optical window of a microscope is limited in size, meaning that while the microscope is focused on a specific area of the micromodel, there is no way to record what is going on in an area that is outside the optical window. A solution is to move the micromodel or the ocular of the microscope rapidly, but this would introduce unknown inertial forces in the micromodel or poor image quality because the camera should be focused at all times, which would be difficult. For quasi-static conditions, this technique is quite appropriate.

Direct Visualization with a Camera

This method is somewhat similar to the setup described above. The difference is that no microscope is used and the camera captures images directly (Soll et al., 1993; Chang et al., 2009a, 2009b;

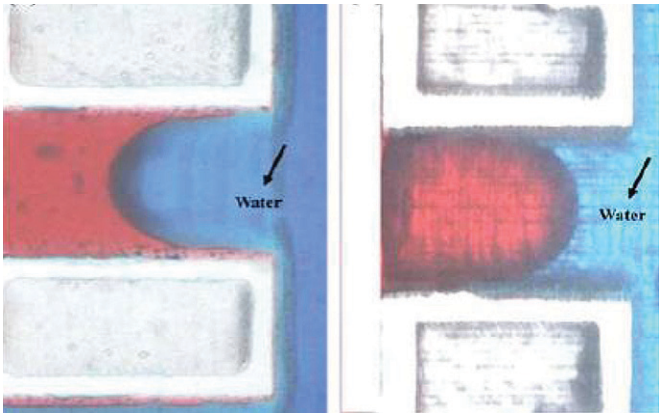

Fig. 17. Photographs taken with a camera (Chang et al., 2009a): a channel from a micromodel (left) and the same channel after treatment to become hydrophilic (right). Diesel fuel is shown in red and the water is blue.

Conrad et al., 1992; Hematpour et al., 2011). Thus the camera can be placed at different orientations with respect to the micromodel. The camera can be situated at a distance from the micromodel to exclude any vibrations affecting the system. The camera may also have an extra objective lens to increase the magnification of the system. High-resolution digital cameras with sophisticated charge coupled device (CCD) and complementary metal-oxide semiconductor (CMOS) sensors allowed the elimination of the microscope.

Figure 17 shows images of an acrylic micromodel taken with a camera at a resolution of 640 by 480 in a red, green, blue (RGB) format (Chang et al., 2009a). The micromodel shown on the right was treated to have a thin film of silicate coating on the acrylic surface. The effect of this treatment on micromodel wettability is quite visible. After heating in an oven at 110°C, the silicate coating changed the wetting characteristics of the micromodel from hydrophobic (left) to hydrophilic (right).

Generally, cameras without a microscope are used to analyze and measure when magnification of the image is not necessary and the needs for resolution are not stringent. The use of a microscope provides better resolution but less flexibility. Currently, cameras built for monitoring micro-phenomena have a satisfying frame rate for photographs and video, as well as good resolution and color depth. Also, powerful software provides easy handling and analysis of the data acquired. Cameras have the advantage of moving without disturbing the micromodel. This offers the ability to monitor dynamic or static effects where the movement of the camera could be necessary. More than one camera can also be used to monitor different parts of a micromodel simultaneously. This cannot be done when using a microscope–camera setup.

Photoluminescent Volumetric Imaging—Confocal Microscopy

Montemagno and Gray (1995) introduced the photoluminescent volumetric imaging (PVI) method. To construct their porous medium, they used optical-quality quartz grains. They used two immiscible fluids, with their refractive indices matched to quartz (Budwig, 1994). The wetting phase was doped with property-selective fluorophores that preferentially partitioned onto the fluid–fluid interface. The system was surveyed with a planar laser source at successive planes. The laser beam excited the fluorophores and thereby illuminated the fluid–fluid interfaces. A CCD camera was used to capture the fluorescent image (Fig. 18). After processing of these images, a three-dimensional data set was generated showing the pore space as well as the location of the fluid–fluid interfaces.

The experimental setup consisted of an Ar-ion laser source emitting at 514.5 nm, a beam expander, a cylindrical lens, the sample cell, a spectral filter, the imaging optics, and a CCD camera. The Ar-ion laser source emitted a laser beam with a diameter of 1.5 mm. The beam expander increased the beam's diameter to 25 mm, and the cylindrical lens transformed the beam from cylindrical to planar. The beam's thickness was 125 μm and had a width of 15 mm in the sample cell. When the fluorophores in the sample cell were excited, they emitted a light with a different wavelength from that of the excitation source. This light passed through a spectral filter, which cut off any unwanted wavelengths, and, with the proper optics, was directed to the CCD camera. After an exposure of approximately 100 ms, the CCD system digitized the image and transferred it to a computer. The resolution gained was better than 1 μm across volumes even greater than 125 mm^3.

As a continuation of the work of Montemagno and Gray, Zang (1998) studied the application of PVI in multiphase dynamics in porous media. Later, Stöhr et al. (2003) used this method to perform three-dimensional measurements of single-phase flow and transport at the pore scale. This method was the first high-resolution index-matching technique to visualize the flow of two immiscible liquids at the same time.

One application of fluorescent microscopy is micro-particle imaging velocimetry (μ-PIV), a technique used to investigate

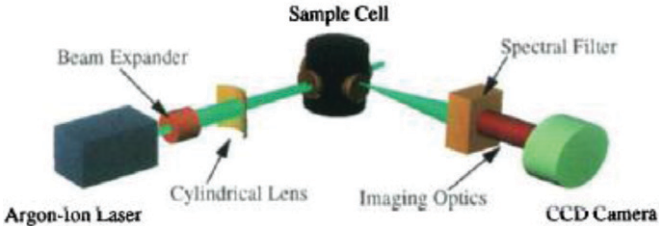

Fig. 18. The experimental setup for photoluminescent volumetric imaging (Montemagno and Gray, 1995).

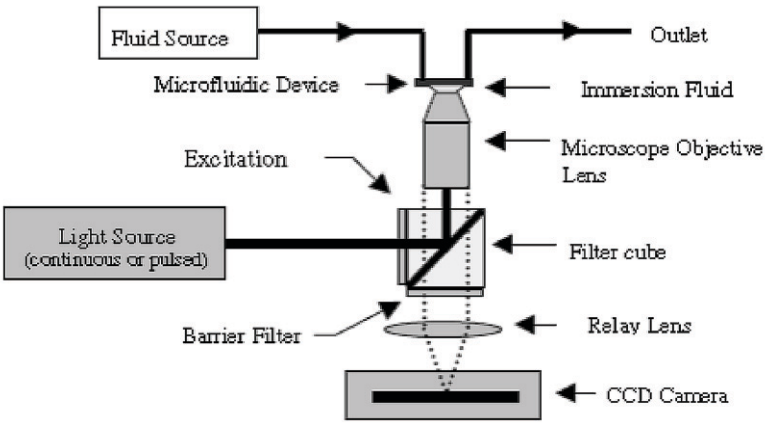

Fig. 19. Schematic description of a typical micro-photoluminescent volumetric imaging hardware implementation (Wereley and Meinhart, 2005).

micrometer-scale fluidic transport and mixing (Shinohara et al., 2004a; Perrin et al., 2005; Fernández Rivas et al., 2008). Micro-PIV has been used to study pressure-driven flow (Meinhart et al., 1999; Tretheway and Meinhart, 2002; Devasenathipathy et al., 2003; Sato et al., 2003; Shinohara et al., 2004b), electro-osmotic flow (Devasenathipathy et al., 2002), and the fluid dynamics of blood capillaries in vivo (Sugii et al., 2002) and in vitro (Sugii and Okamoto, 2004; Okuda et al., 2003).

Micro-PIV is based on the particle imaging velocimetry method, where micrometer-size particles are used as markers in fluid flow to measure instantaneous velocity fields in experimental fluid mechanics (Keane and Andrian, 1992). These particles should match well the properties of the fluid under consideration; they should follow the movement of the fluid, should not affect its properties (such as viscosity), and should not sink. Lindken et al. (2009) presented a review of μ-PIV including recent developments, applications, and guidelines.

Wereley and Meinhart (2005) gave a detailed description of the technique in theory and practice. Figure 19 shows a schematic description of a typical μ-PIV hardware implementation.

The imaging principle is fluorescent microscopy. The laser source, which can be pulsed or continuous wave, emits light that is guided to a lens that converts the light beam to a planar one. Light passing through the micromodel excites the fluorescent particles, and when they get de-excited, they emit light at a higher wavelength. The filter allows only light emitted from the fluorescent particles to reach the camera's sensor. To increase the efficiency of the technique, the objective of the microscope is put into immersion oil.

In this way, two-dimensional images can be obtained. Three-dimensional images can be constructed if fluorescent microscopy is combined with confocal microscopy. From these images, the change in the position of an individual particle can be measured.

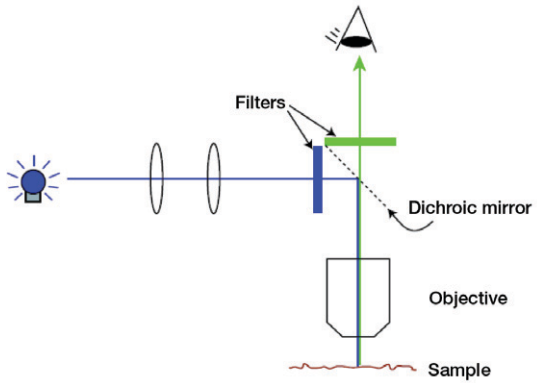

Fig. 20. The basic setup for confocal microscopy (Semwogerere and Weeks, 2005).

Because the time interval between two sequential images is known, the whole velocity field can be computed. If the particles are property selective, the flow velocity of individual phases can be measured using different particles for different phases.

Confocal microscopy is another technique based on the same effect (laser-induced fluorescence) but is applied differently. It is a point-by-point imaging method. Confocal microscopy creates sharp images of specimens that would otherwise appear blurred when viewed with a conventional microscope. It also allows the construction of a three-dimensional image of the specimen by superposing two-dimensional images obtained at sequential layers. Marvin Minsky patented confocal microscopy in 1957 (Minsky, 1988). Semwogerere and Weeks (2005) presented the basic concepts of confocal microscopy.

Figure 20 provides a schematic of confocal microscopy (Semwogerere and Weeks, 2005). Light from a monochromatic light source (usually a laser) is reflected from a dichroic mirror and projected onto the specimen through an objective lens. The sample is either dyed with fluorescent dyes or contains fluorescent particles. These particles

Table 2. The visualization methods along with their limitations and their applicability.

Visualization method	Suitability	Limitations
Microscope and camera	any transparent (partially) two-dimensional micromodel, high-resolution optical image	not suitable for three-dimensional models, limited in resolution (>1 μm)
Direct visualization with a camera	relaxed needs in resolution, high acquisition rate	not suitable for three-dimensional models, very low resolution
Photo-luminescent volumetric imaging	three-dimensional porous media, high resolution	refractive index matching is necessary, relatively slow effects, relatively expensive
Confocal microscopy	very high resolution (submicron), quasi-static or very low speed effects	effective for depths up to 250 μm, relatively expensive, very low acquisition rate, not suitable for dynamic effects

absorb the light from the light source and emit light when they get de-excited at a wavelength that is higher than the absorbed light. This emitted light passes through the dichroic mirror while the light from the light source is reflected back to the source. Two filters are used to ensure that only light that is along the optical axis will be used. Thus, the sample is visualized point by point in two dimensions.

Confocal microscopy is ideal for effects that are relatively slow and where the smallest feature that needs to be visualized is less than the optical diffraction limit—precisely where conventional optical microscopy fails to give results (Lindek et al., 1996; Hell et al., 1994; Baumann and Werth, 2004; Baumann et al., 2002; Baumann, 2007; Sirivithayapakorn and Keller, 2003; Keller and Auset, 2007; Baumann and Niessner, 2006; Wan and Wilson, 1994a, 1994b). Grate et al. (2010) discussed the visualization of wetting film structures and a nonwetting immiscible fluid in a pore network micromodel using a solvatochromic dye.

In Table 2, the visualization methods along with their limitations and applicability are presented.

Applications of Micromodels in Studies of Flow and Transport in Porous Media

Studies of Two-Phase Displacement Processes

The majority of the applications of micromodels in studies of flow and transport in porous media are related to the immiscible displacement of two fluid phases (Avraam et al., 1994; Baouab et al., 2007; Dawe et al., 2010, 2011; Budwig, 1994; Chatenever and Calhoun, 1952; Chen and Wilkinson, 1985; Chuoke et al., 1959; Corapcioglu et al., 2009; Coskuner, 1997; Cottin et al., 2011; Crandall et al., 2009; de Zélicourt et al., 2005; Tóth et al., 2007; Tsakiroglou and Avraam, 2002; van der Marck and Glas, 1997; Wan et al., 1996; Chang et al., 2009a, 2009b; Theodoropoulou et al., 2005; Berejnov et al., 2008; Tsakiroglou et al., 2003a, 2003b, 2007). Processes of drainage and imbibition, as well as the mechanisms that dominate them, like viscous or capillary fingering, snap-off, etc., have been studied using micromodels (Zhang et al., 2011a, 2011b; Ferer et al., 2004; Grate et al., 2010; Gutiérrez et al., 2008; Hug et al., 2003; Huh et al., 2007; Jeong and Corapcioglu, 2003, 2005; Jeong et al., 2000; Lovoll et al., 2005; Mattax and Kyte, 1961; Montemagno and Gray, 1995; Pyrak-Nolte et al., 1988; Rangel-German and Kovscek, 2006; Stöhr et al., 2003; Sugii and Okamoto, 2004; Tallakstad et al., 2009; Lenormand and Zarcone, 1985a, 1985b; Lenormand, 1989a, 1989b; Lenormand et al., 1988; Sharma et al., 2011; Romano et al., 2011; Frette et al., 1997).

One of the first studies of two-phase flow under quasi-static conditions and the relevant displacement mechanisms was presented in the work of Lenormand et al. (1983). They used a transparent polyester resin micromodel (Bonnet and Lenormand, 1977), with the channels in the form of a network of capillary ducts. They observed the displacement of the meniscus formed by the two phases under different conditions, like piston-type motion and snap-off. They determined that two types of imbibition can occur depending on the number and spacing of the ducts filled with the nonwetting phase. Later on, Chang et al. (2009b) conducted displacement experiments following Lenormand's assumptions. They provided valuable experimental support and suggestions for Lenormand's displacement formulas, which are the basis for many related experimental and numerical studies. Lovoll et al. (2010) used a glass-bead micromodel to study the influence of viscous fingering on dynamic saturation–pressure curves. They obtained a scaling relation between pressure, saturation, system size, and the capillary number.

Dong and Chatzis (2010) studied the movement of a wetting film in a liquid–gas system. They used a consolidated glass-bead micromodel. They found that the capillary pressure controls the wetting film imbibition ahead of the main displacement front.

Cottin et al. (2010) studied the transition from capillary to viscous flow during drainage and its dependence on the capillary number. They used two kinds of micromodels. One was manufactured using standard soft-lithography techniques and the other was manufactured with wet-etching techniques. Their experiments shed light on the role of viscous forces during the invasion process and their competition with the capillary force. At very low applied capillary number, the invading liquid flowed through one single channel at the time and built a very open structure. At larger capillary number, the role of viscous forces increased.

Measurements of Interfacial Area and Phase Saturation

An important application of micromodels has been in the measurement of two-phase flow properties that cannot be determined with standard experiments. A major example is the quantification

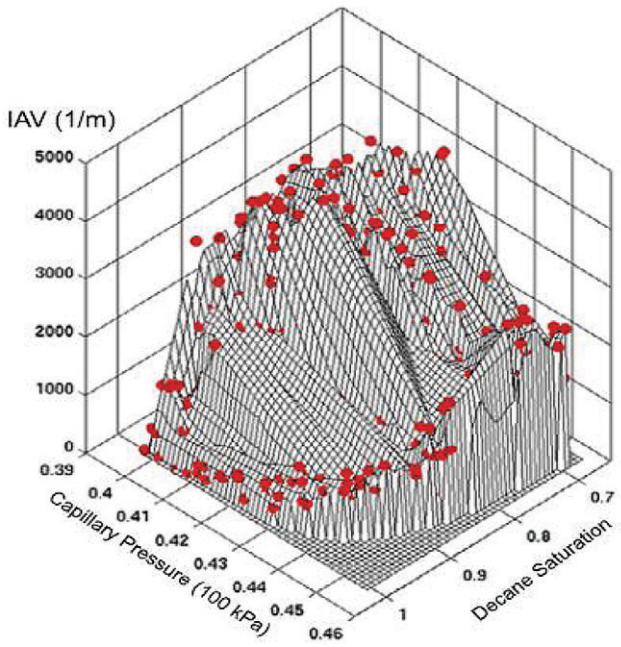

Fig. 21. Graphical representation of the phase saturation, capillary pressure, and interfacial area per volume (IAV) triplets (in red) during drainage experiments (Cheng et al., 2004).

of the area of interfaces formed between phases, in particular the fluid–fluid interface. The significance of fluid–fluid interfaces in two-phase flow was recognized as early as 1951. Rapoport and Leas (1951) elucidated the role of interfaces and interfacial energies in controlling the simultaneous flow of two fluids in a porous medium. Later on, theoretical studies proposed that a complete description of two-phase flow in a porous medium should take into account the evolution and dynamics of fluid–fluid interfaces (see, e.g., Marle, 1981, 1982; Hassanizadeh and Gray, 1990, 1993a, 1993b). A major obstacle to making advances in this regard is our ability to measure the specific interfacial area. Micromodels have made possible the experimental investigation of the role of interfaces (Crandall et al., 2010; Pyrak-Nolte et al., 2008).

Recently, two-phase flow studies were performed using photoresist micromodels that had flow patterns based on stratified percolation (Cheng, 2002; Pyrak-Nolte et al., 2008; Cheng et al., 2004; Chen et al., 2007). In these studies, distributions of the two phases in the flow network during quasi-static drainage and imbibition were visualized. Phase saturation and interfacial area could be determined using image processing, and the relationships among phase saturation, capillary pressure, and interfacial area were investigated. It was found that for each set of capillary pressure and saturation data points, a single value for the specific interfacial area exists (see Fig. 21). More importantly, the surfaces produced by the graphical representation of these triplets were nearly the same for drainage and imbibition, within the limits of experimental error (Chen et al., 2007; Cheng, 2002; Cheng et al., 2004; Liu et al., 2011). Later, dynamic drainage and imbibition displacement experiments were performed (Bottero, 2009; Crandall et al., 2010). Under these conditions, unlike qualitative experiments, capillary pressure within the network is no longer equal to the externally applied pressure. Therefore, the local capillary pressure was determined from the curvature of each individual interface.

In these visualizations, interfaces are seen as a line and there is no information on the third dimension. If the depth of the model is assumed to be constant, the area of interfaces can be calculated. The depth of a photoresist model, however, is not really constant. The photoresist layer where the flow network lies is produced by spin-coating. Because centrifugal forces depend on the distance from the origin, the depth of the model is not the same everywhere. This discrepancy can be negligible, however, in small micromodels.

The curvature of an interface in the third direction cannot be determined by optical means. If images are acquired in grayscale and a very high resolution, the curvature may be estimated by means of processing the change in the gray shade of the interface.

If only the quasi-static case is examined, fluorescent microscopy could present an alternative to optical means to obtain three-dimensional images. In this case, the model should be very small in size (a few pores), given that the field of view is limited. Under dynamic conditions, conventional optical microscopy is the best way to deal with the situation. Any other method requires time for image acquisition. During this time, the distribution of phases in the flow network changes in a way that makes the images acquired useless.

Measurements of Relative Permeability

The effective two-phase flow coefficients of porous media, such as the capillary pressure and relative permeability functions, bridge the gap between the microscopic flow dynamics and the macroscopic behavior of porous media flow (Kalaydjian, 1990; Avraam and Payatakes, 1999; Chang et al., 2009a; Rapoport and Leas, 1951; Tsakiroglou et al., 2005, 2003a, 2007; Wang et al., 2006). Thus determining relative permeability of each phase as a function of saturation under a wide range of experimental conditions is important (Chang et al., 2009a). Tsakiroglou et al. (2003a) used micromodels to study the influence of the capillary number on nonequilibrium immiscible displacement in two-phase flow experiments. They showed that the relative permeabilities of the two phases not only are a function of saturation but also strongly depend on capillary numbers (Fig. 22).

Tsakiroglou et al. (2003a) performed their measurements with a glass-etched micromodel, initially totally filled with the wetting phase (distilled water with methylene blue). The nonwetting phase (paraffin oil) was then injected into the network at a fixed flow rate with the use of a syringe pump. With the use of a CCD camera, successive shots of the displacement were captured from a central region of the network. The pressure drop along this central

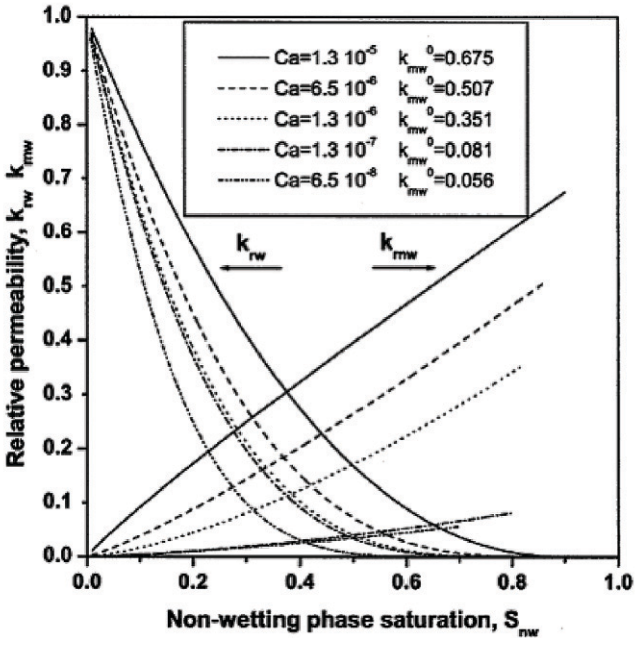

Fig. 22. Estimated relative permeability–saturation curves for different capillary numbers (Ca) (Tsakiroglou et al., 2003a).

region of the network with respect to time was measured with a differential pressure transducer. This procedure allowed the determination of the saturation and relative permeability of each phase as a function of time.

Alternatively, Chang et al. (2009a) calculated relative permeability by keeping a constant pressure head difference between the wetting and the nonwetting phases. For drainage, the nonwetting phase was introduced into a micromodel that was already fully saturated with the wetting phase, while the wetting phase flow rate was measured. This was continued until steady state was reached. Images from the micromodel were taken with the use of a CCD camera.

The main issue that needs to be addressed in such measurements is the accuracy in determining phase pressures or in measuring phase saturation. Phase saturation measurement depends on the resolution of the visualization setup and can usually be quantified. Phase pressure, however, is very difficult to measure. Especially in complex flow networks with very small dimensions, it is practically impossible to measure local pressure within the micromodel. Postprocessing is necessary to retrieve and calculate the average value for a given spatial domain.

Enhanced Oil Recovery

Micromodels have also been used to study oil recovery from underground reservoirs in the presence of gas and water phases (Keller et al., 1997). Buckley (1990) reviewed the application of micromodels in multiphase flow and enhanced oil recovery. Enhanced oil recovery relies on the displacement of oil by another liquid or gas toward a well where the oil is collected (Liu, 2006). The most common techniques involve the injection of gases and chemicals, such as polymers and foams. The success of these techniques depends on the physical properties of each phase, the viscosity ratios, capillary number, temperature, reservoir conditions, and flow dynamics. These factors have been studied in a number of micromodels (Amani et al., 2010; Armstrong and Wildenschild, 2012; Dong et al., 2007; Hematpour et al., 2011; Nguyen et al., 2002; Nourani et al., 2007; Sagar and Castanier, 1998; Soudmand-asli et al., 2007; Wyckoff and Botset, 1936; Zekri and El-Mehaideb, 2002; Mahers and Dawe, 1985; Wardlaw, 1980; Bora et al., 1997; Nguyen et al., 2002; Lago et al., 2002; Hornbrook et al., 1991; Romero et al., 2002; Sohrabi et al., 2001, 2004; Feng et al., 2004; van Dijke et al., 2002; Liu et al., 2002; Liu, 2006; Oren et al., 1992; Sayegh and Fisher, 2008; Doorwar and Mohanty, 2011; Wang et al., 2006; Naderi and Babadagli, 2011).

Dong et al. (2007) used a micromodel to investigate the displacement mechanisms of alkaline flooding in enhanced heavy oil recovery (EOR). They observed that two mechanisms govern the EOR process. One was in situ water-in-oil (W/O) emulsion and partial wettability alteration; the other was the formation of an oil-in-water (O/W) emulsion. Heavy oil was emulsified in brine by an alkaline plus a very dilute surfactant formula, entrained in the water phase, and produced out of the model. The upper left image in Fig. 23 shows the micromodel containing heavy oil and irreducible water at the end of oil injection. The upper right section is an image of pore-level oil and water distribution. This image shows water films surrounding the solid boundaries and the continuous oil phase staying in the central portion of pores and throats of

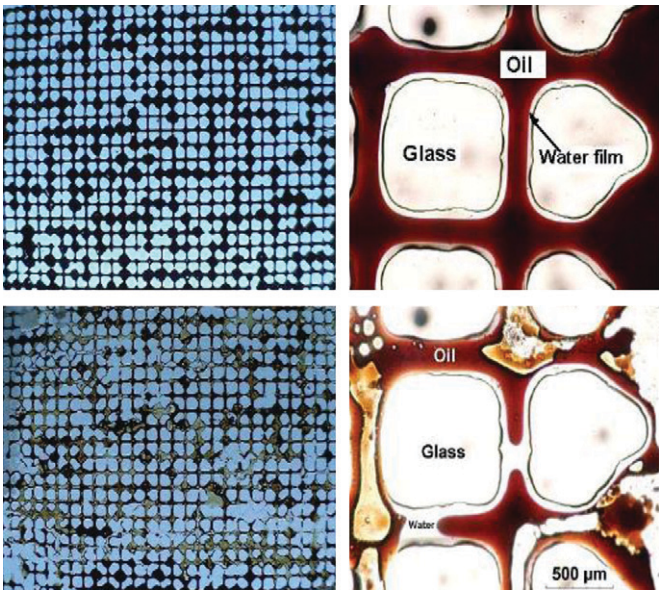

Fig. 23. Micromodel with heavy oil and irreducible water saturation: portions of the micromodel (left) and pore-level images of the formation of a water–oil emulsion in alkaline injection (right) (Dong et al., 2007).

the pore network. The image also shows that the micromodel is water wet. The lower part of Fig. 23 shows the micromodel network with an injection of a chemical slug. In this alkaline injection, the injected water phase penetrated into the residual oil phase and created some discontinuous water ganglia inside the oil channels to form a W/O emulsion. The viscosity of the W/O emulsion was much higher than that of the crude oil. Therefore, the oil was displaced in the form of a W/O emulsion with little fingering effect. Some oil also touched the pore walls, indicating that the pore wall became partially oil wet. The wettability alteration also aided in blocking the water flow in those channels.

Nourani et al. (2007) used a glass micromodel to simulate a fractured system and the microbial-enhanced oil recovery (MEOR) technique (Stewart and Fogler, 2001, 2002; Soudmand-asli et al., 2007; Armstrong and Wildenschild, 2010; Amani et al., 2010; Zekri and El-Mehaideb, 2002). This method is based on the reduction of interfacial tension and the change in the wettability of rock with the aid of bacteria to make the displacement of oil easier. In their work, Nourani et al. (2007) took five bacterial species from crude oil originating from one of the aging Persian fractured reservoirs. These microorganisms are very good at increasing oil recovery in the two ways mentioned above. Two series of visualization experiments were performed to examine the behavior of MEOR in micromodels designed to resemble the fractured system: static and dynamic. In the static experiments, a carbonate rock–glass micromodel was used to simulate the reservoir conditions. The dynamic experiments were performed in a glass micromodel that had a fracture with a 45° inclination. The image processing methodology was used to determine the recovery achieved by MEOR in the micromodel made of glass.

Summary and Discussion

This review of micromodels presented the most important concepts behind choosing a flow network in a micromodel, the different manufacturing techniques of micromodels, the available visualization methods, and the various applications of micromodels.

The flow networks used in micromodels can be classified based on the model structure and the statistical distribution of sizes assigned to its features. The pattern chosen, the size distribution of its features, and the experimental purpose determine the choice of the micromodel's fabrication method. Wet-etching techniques that are isotropic create a curvature on the walls of the micromodel. If optical microscopy with back-light illumination is used, this curvature on the walls may cause severe problems. It causes refraction, and the images at the bottoms of channels are shown in black. A possible, but not entirely effective, solution is to use a light diffuser. While dry-etching techniques, like plasma etching, provide vertical walls, they are not that efficient when the micromodel becomes deep. It is very difficult to reach depths $\geq$50 μm without damaging the profile of the channel or the verticality of the walls.

An inexpensive and effective way of making micromodels is optical lithography. It is accurate and precise; however, it has a major drawback. If the photoresist, inside which micromodel channels are made, is exposed to UV or near-UV light, then it produces N_2 that will eventually destroy the model on its way out of the closed system. A solution to this problem is to hard bake the model before using it or use filters that partially block the harmful wavelengths. None of these solutions are permanent, however. The only effective solution is to totally eliminate wavelengths close to the harmful spectral region, which could be quite expensive.

Stereo lithography is an effective way of making polymeric micromodels provided that they are not very small. This technique is effective in manufacturing integrated structures, but it becomes problematic when the dimensions become very small (micrometers). Moreover, stereo lithography is expensive because an integrated commercial system is needed to produce such models.

Soft lithography is an inexpensive and effective way of making polymeric micromodels. The major problem with these models, when it comes to flow studies, is that their wetting properties change with time. After some time, the wetting phase may become the nonwetting phase. Also, care must be taken to ensure that the phases involved in two-phase flow experiments will not cause the material to swell or become deformed.

Hele–Shaw and glass-bead models are easy to make without spending too much time and money. They are useful and simple; however, they have problems being visualized optically. The beads or spheres between the two glass plates limit visualization to only one side because they are three-dimensional objects. As such, measurements of saturation or the interfacial area will not be accurate enough and some assumptions regarding the symmetry of the menisci must be made.

All manufacturing methods requiring a mask are highly affected by the preciseness of the mask used to form the network on the material. If the mask is of low resolution, then the actual network will be of low resolution, too.

Various ways of visualizing events occurring in a micromodel include using a camera, combining a microscope and a camera, and laser-induced fluorescence. The use of a microscope, with or without a camera, is a purely optical way of visualizing flow through the micromodels. The accuracy of measurement is highly dependent on the resolution of the recording apparatus, which is always lower than the diffraction limit. Laser-induced fluorescence methods are more accurate. With their use, three-dimensional images can be reconstructed, which cannot be done with optical means. These methods are restricted, however, in their acquisition time and their field of view. Thus, they can be used only under static, or nearly static, conditions. In the case of front-light optical microscopy, the flow network can be formed in silicon and sealed with glass or

another transparent material. This would introduce wettability issues, however, because the phases involved will experience the presence of two different materials with different wetting properties, something that is not desired. Evidently, deciding on the appropriate micromodel for a specific application is complicated.

Micromodels have been and will continue to be a very powerful tool to study flow and transport phenomena on the microscale. Further research is needed, however, to improve their properties, the existing techniques of manufacturing and visualization, as well as the development of new materials and techniques. For instance, one of the limiting factors in the use of micromodels in two-phase flow is the optical visualization of flow and the distribution of fluids in three-dimensional micromodels. This is important in the sense that single-layered micromodels are considered to be quasi-two-dimensional porous media. This raises some questions regarding their correspondence to real porous media. The improvement of etching methods so as to create channels that have a rectangular cross-section at depths >40 μm is also a challenge. Another important issue is the development of microsensors for measuring the local phase pressure within the flow network of a micromodel; this will be a major advantage in two-phase flow studies. Also, the development of new materials or the modification of the existing ones is needed to meet certain experimental requirements. For example, for reliable and accurate experimental results, it is important to have micromodels with stable wetting properties. Finally, the ultimate goal would be to have the ability to produce cheap, easy-to-make micromodels that represent a real porous medium well and to be able to take measurements that can be trusted, independently of the nature of the model, in terms of their dimensions.

Acknowledgments

This work was funded by the Netherlands Organisation for Scientific Research (NWO), under Grant no. 818.01.008. We are members of the International Research Training Group NUPUS, financed by the German Research Foundation (DFG) (Grant no. GRK 1398) and NWO (Grant no. DN 81-754). We appreciate critical comments by two anonymous referees, which helped to improve the manuscript.

References

Amani, H., M.H. Sarrafzadeh, M. Haghighi, and M.R. Mehrnia. 2010. Comparative study of biosurfactant producing bacteria in MEOR applications. J. Pet. Sci. Eng. 75:209–214. doi:10.1016/j.petrol.2010.11.008

Armstrong, R.T., and D. Wildenschild. 2010. Designer-wet micromodels for studying potential changes in wettability during microbial enhanced oil recovery. Poster presented at: American Geophysical Union Fall Meeting, San Francisco. 13–17 Dec. 2010. Abstr. H53D-1061.

Armstrong, R.T., and D. Wildenschild. 2012. Microbial enhanced oil recovery in fractional-wet systems: A pore-scale investigation. Transp. Porous Media 92:819–835. doi:10.1007/s11242-011-9934-3

Arnold, J., U. Dasbach, W. Ehrfeld, K. Hesch, and H. Löwe. 1995. Combination of excimer laser micromachining and replication processes suited for large scale production. Appl. Surf. Sci. 86:251–258. doi:10.1016/0169-4332(94)00386-6

Auset, M., and A.A. Keller. 2004. Pore-scale processes that control dispersion of colloids in saturated porous media. Water Resour. Res. 40:W03503. doi:10.1029/2003WR002800

Avraam, D.G., G.B. Kolonis, T.C. Roumeliotis, G.N. Constantinides, and A.C. Payatakes. 1994. Steady-state two-phase flow through planar and nonplanar model porous media. Transp. Porous Media 16:75–101. doi:10.1007/BF01059777

Avraam, D.G., and A.C. Payatakes. 1999. Flow mechanisms, relative permeabilities, and coupling effects in steady-state two-phase flow through porous media: The case of strong wettability. Ind. Eng. Chem. Res. 38:778–786. doi:10.1021/ie980404o

Baouab, Z., M. Najjari, H. Ouerfelli, and S. Ben Nasrallah. 2007. Experimental study of the effects of hydraulic gradient and injected-gas flow rate on fragmentation in porous media. J. Pet. Sci. Eng. 59:250–256. doi:10.1016/j.petrol.2007.04.009

Basov, N.G., V.A. Danilychev, Y.M. Popov, and D.D. Khodkevich. 1970. Laser operating in the vacuum region of the spectrum by excitation of liquid Xe by an electron beam. JETP Lett. 12:329.

Baumann, T. 2007. Colloid transport processes: Experimental evidence from the pore scale to the field scale. In: F.H. Frimmel et al., editors, Colloidal transport in porous media. Springer-Verlag, Berlin. p. 55–86.

Baumann, T., and R. Niessner. 2006. Micromodel study on repartitioning phenomena of a strongly hydrophobic fluorophore at a colloid/1-octanol interface. Water Resour. Res. 42:W12S04. doi:10.1029/2006WR004893

Baumann, T., and C.J. Werth. 2004. Visualization and modeling of polystyrol colloid transport in a silicon micromodel. Vadose Zone J. 3:434–443. doi:10.2136/vzj2004.0434

Baumann, T., C.J. Werth, and R. Niessner. 2002. Visualisation of colloid transport processes with magnetic resonance imaging and in etched silicon micromodels. DIAS Rep. Plant Prod. 80:25–30.

Berejnov, V., N. Djilali, and D. Sinton. 2008. Lab-on-chip methodologies for the study of transport in porous media: Energy applications. Lab Chip 8:689–693. doi:10.1039/b802373p

Blauw, M.A., T. Zijilstr, and E. van der Drift. 2001. Balancing the etching and passivation in time-multiplexed deep dry etching of silicon. J. Vac. Sci. Technol. B 19:2930–2934. doi:10.1116/1.1415511

Blunt, M., and P. King. 1991. Relative permeabilities from two- and three-dimensional pore-scale network modelling. Transp. Porous Media 6:407–433. doi:10.1007/BF00136349

Bonnet, J., and R. Lenormand. 1977. Realisation de micromodeles pour l'etude des ecoluments polyphasiques en milieu poreux. Rev. Inst. Fr. Pet. 42:477–480.

Bora, R., B.B. Maini, and A. Chakma. 1997. Flow visualization studies of solution gas drive process in heavy oil reservoirs using a glass micromodel. Paper presented at: SPE International Thermal Operations and Heavy Oil Symposium, Bakersfield, CA. 10–12 Feb. 1997. Paper 37519-MS.

Bottero, S. 2009. Advances in the theory of capillarity in porous media. Ph.D. diss. Utrecht Univ., Utrecht, the Netherlands.

Buckley, J.S. 1990. Multiphase displacements in micromodels. In: N.R. Morrow, editor, Interfacial phenomena in oil recovery. Marcel Dekker, New York. p. 157–189.

Budwig, R. 1994. Refractive index matching methods for liquid flow investigations. Exp. Fluids 17:350–355. doi:10.1007/BF01874416

Chang, L.-C., Z.H.-H. Chen, and H.-Y. Shan. 2009a. Effect of connectivity and wettability on the relative permeability of NAPLs. Environ. Geol. 56:1437–1447. doi:10.1007/s00254-008-1238-8

Chang, L.-C., J.-P. Tsai, H.-Y. Shan, and H.-H. Chen. 2009b. Experimental study on imbibition displacement mechanisms of two-phase fluid using micro model. Environ. Earth Sci. 59:901–911. doi:10.1007/s12665-009-0085-6

Chatenever, A., and J.C. Calhoun, Jr. 1952. Visual examinations of fluid behavior in porous media: Part 1. J. Pet. Technol. 4:149–156. doi:10.2118/135-G

Chen, D., L.J. Pyrak-Nolte, J. Griffin, and N.J. Giordano. 2007. Measurement of interfacial area per volume for drainage and imbibitions. Water Resour. Res. 43:W12504. doi:10.1029/2007WR006021

Chen, J.-D., and D. Wilkinson. 1985. Pore-scale viscous fingering in porous media. Phys. Rev. Lett. 55:1892–1895. doi:10.1103/PhysRevLett.55.1892

Cheng, J.-T. 2002. Fluid flow in ultra-small capillaries. Ph.D. diss. Purdue Univ., West Lafayette, IN.

Cheng, J.-T., and N.J. Giordano. 2002. Fluid flow through nanometer-scale channels. Phys. Rev. E 65:031206. doi:10.1103/PhysRevE.65.031206

Cheng, J.-T., L.J. Pyrak-Nolte, D.D. Nolte, and N.J. Giordano. 2004. Linking pressure and saturation through interfacial areas in porous media. Geophys. Res. Lett. 31:L08502. doi:10.1029/2003GL019282

Chuoke, R.L., P. van Meurs, and C. van der Poel. 1959. The instability of slow, immiscible, viscous liquid–liquid displacements in permeable media. Trans. Am. Inst. Min. Metall. Pet. Eng. 216:188–194.

Conrad, S.H., J.L. Wilson, W.R. Mason, and W.J. Peplinski. 1992. Visualization of residual organic liquids trapped in aquifers. Water Resour. Res. 28:467–478. doi:10.1029/91WR02054

Corapcioglu, M.Y., S. Chowdhury, and S.E. Roosevelt. 1997. Micromodel visualization and quantification of solute transport in porous media. Water Resour. Res. 33:2547–2558. doi:10.1029/97WR02115

Corapcioglu, M.Y., and P. Fedirchuk. 1999. Glass bead micromodel study of solute transport. J. Contam. Hydrol. 36:209–230. doi:10.1016/S0169-7722(98)00145-4

Corapcioglu, M.Y., S. Yoon, and S. Chowdhury. 2009. Pore-scale analysis of NAPL blob dissolution and mobilization in porous media. Transp. Porous Media 79:419–442. doi:10.1007/s11242-008-9331-8

Coskuner, G. 1997. Microvisual study of multiphase gas condensate flow in porous media. Transp. Porous Media 28:1–18. doi:10.1023/A:1006505706431

Cottin, C., H. Bodiguel, and A. Colin. 2010. Drainage in two-dimensional porous media: From capillary to viscous flow. Phys. Rev. E 82:046315. doi:10.1103/PhysRevE.82.046315

Cottin, C., H. Bodiguel, and A. Colin. 2011. Influence of wetting conditions on drainage in porous media: A microfluidic study. Phys. Rev. E 84:026311. doi:10.1103/PhysRevE.84.026311

Crandall, D., G. Ahmadi, M. Ferer, and D.H. Smith. 2009. Distribution and occurrence of localized-bursts in two-phase flow through porous media. Physica A 388:574–584. doi:10.1016/j.physa.2008.11.010

Crandall, D., G. Ahmadi, D. Leonard, M. Ferer, and D.H. Smith. 2008. A new stereolithography experimental porous flow device. Rev. Sci. Instrum. 79:044501. doi:10.1063/1.2903740

Crandall, D., G. Ahmadi, D.H. Smith, and G. Bromhal. 2010. Direct, dynamic measurement of interfacial area within porous media. In: 7th International Conference on Multiphase Flow: ICMF 2010 Proceedings, Tampa, FL. 30 May–4 June 2010. Univ. of Florida, Gainesville. Paper 10.3.2.

Dawe, R.A., A. Caruana, and C.A. Grattoni. 2010. Microscale visual study of end effects at permeability discontinuities. Transp. Porous Media 86:601–616. doi:10.1007/s11242-010-9642-4

Dawe, R.A., A. Caruana, and C.A. Grattoni. 2011. Immiscible displacement in cross-bedded heterogeneous porous media. Transp. Porous Media 87:335–353. doi:10.1007/s11242-010-9687-4

Devasenathipathy, S., J.G. Santiago, and K. Takehara. 2002. Particle tracking techniques for electrokinetic microchannel flows. Anal. Chem. 74:3704–3713. doi:10.1021/ac011243s

Devasenathipathy, S., J.G. Santiago, S.T. Wereley, C.D. Meinhart, and K. Takehara. 2003. Particle imaging techniques for microfabricated fluidic systems. Exp. Fluids 34:504–514.

de Zélicourt, D., K. Pekkan, H. Kitajima, D. Frakes, and A.P. Yoganathan. 2005. Single-step stereolithography of complex anatomical models for optical flow measurements. J. Biomech. Eng. 127:204–207. doi:10.1115/1.1835367

Dong, M., and I. Chatzis. 2010. Effect of capillary pressure on wetting film imbibition ahead of main liquid–gas displacement front in porous media. Pet. Sci. Technol. 28:955–968. doi:10.1080/10916460902937067

Dong, M., Q. Liu, and A. Li. 2007. Micromodel Study of the displacement mechanisms of enhanced oil recovery by alkaline flooding. Paper presented at: International Symposium of the Society of Core Analysts, Calgary, AB, Canada. 10–12 Sept. 2007. Paper SCA 2007-47.

Doorwar, S., and K.K. Mohanty. 2011. Viscous fingering during non-thermal heavy oil recovery. Paper presented at: SPE Annual Technical Conference and Exhibition, Denver, CO. 30 Oct.–2 Nov. 2011. Paper 146841-MS.

Durandet, A., O. Joubert, J. Pelletier, and M. Pichot. 1990. Effects of ion bombardment chemical reaction on wafer temperature during plasma etching. J. Appl. Phys. 67:3862–3866. doi:10.1063/1.345009

Ehrfeld, W., M. Abraham, U. Ehrfeld, M. Lacher, and H. Lehr. 1994. Materials for LIGA products. In: MEMS '94: Proceedings of the IEEE Workshop on Micro Electro Mechanical Systems, Kanagawa, Japan. 25–28 Jan. 1994. IEEE, New York. p. 86–90.

Ehrfeld, W., P. Bley, F. Goetz, P. Hagmann, A. Maner, J. Mohr, et al. 1987. Fabrication of microstructures using the LIGA process. In: K.J. Gabriel and W.S.N. Trimmer, editors, Proceedings of the IEEE Micro Robots and Teleoperators Workshop, Hyannis, MA. 9–11 Nov. 1987. IEEE, Piscataway, NJ. Paper TH02404-8.

Ehrfeld, W., H. Lehr, F. Michel, A. Wolf, H.-P. Gruber, and A. Bertholds. 1996. Microelectro discharge machining as a technology on micromachining. Proc. SPIE 2879:332–337. doi:10.1117/12.251221

Feng, Q.-x., L.-c. Di, G.-q. Tang, Z.-y. Chen, X.-l. Wang, and J.-x. Zou. 2004. A visual micro-model study: The mechanism of water alternative gas displacement in porous media. Paper presented at: SPE/DOE Symposium on Improved Oil Recovery, Tulsa, OK. 17–21 April 2004. Paper 89362-MS. doi:10.2118/89362-MS

Ferer, M., C. Ji, G.S. Bromhal, J. Cook, G. Ahmadi, and D.H. Smith. 2004. Crossover from capillary fingering to viscous fingering for immiscible unstable flow: Experiment and modeling. Phys. Rev. E 70:016303. doi:10.1103/PhysRevE.70.016303

Fernández Rivas, D., M.N. Kashid, D.W. Agar, and S. Turek. 2008. Slug flow capillary microreactor: Hydrodynamic study. Afr. Phys. Rev. 1(Spec. Iss.):0005.

Frette, O.I., K.J. Maloy, and J. Schmittbuhl. 1997. Immiscible displacement of viscosity matched fluids in two dimensional porous media. Phys. Rev. E 55:2969–2975. doi:10.1103/PhysRevE.55.2969

Fritz, J.L., and M.J. Owen. 1995. Hydrophobic recovery of plasma-treated polydimethylsiloxane. J. Adhes. 54:33–45. doi:10.1080/00218469508014379

Gervais, T., J. El-Ali, A. Günther, and K.F. Jensen. 2006. Flow-induced deformation of shallow microfluidic channels. Lab Chip 6:500–507. doi:10.1039/b513524a

Giordano, N., and J.-T. Cheng. 2001. Microfluid mechanics: Progress and opportunities. J. Phys.: Condens. Matter 13:R271. doi:10.1088/0953-8984/13/15/201

Grate, J.W., C. Zhang, T.W. Wietsma, M.G. Warner, N.C. Anheier, Jr., B.E. Bernacki, et al. 2010. A note on the visualization of wetting film structures and a nonwetting immiscible fluid in a pore network micromodel using a solvatochromic dye. Water Resour. Res. 46:W11602. doi:10.1029/2010WR009419

Gutiérrez, B., F. Juarez, L. Ornelas, S. Zeppieri, and A. López de Ramos. 2008. Experimental study of gas–liquid two-phase flow in glass micromodels. Int. J. Thermophys. 29:2126–2135. doi:10.1007/s10765-007-0305-9

Hassanizadeh, S.M., and W.G. Gray. 1990. Mechanics and thermodynamics of multiphase flow in porous media including interphase boundaries. Adv. Water Resour. 13:169–186. doi:10.1016/0309-1708(90)90040-B

Hassanizadeh, S.M., and W.G. Gray. 1993a. Thermodynamic basis of capillary pressure in porous media. Water Resour. Res. 29:3389–3405. doi:10.1029/93WR01495

Hassanizadeh, S.M., and W.G. Gray. 1993b. Toward an improved description of the physics of two-phase flow. Adv. Water Resour. 16:53–67. doi:10.1016/0309-1708(93)90029-F

Hedlund, C., H.O. Blom, and S. Berg. 1994. Microloading effect in reactive ion etching. J. Vac. Sci. Technol. A 12:1962–1965. doi:10.1116/1.578990

Heiba, A.A., M. Sahimi, L.E. Scriven, and H.T. Davis. 1992. Percolation theory of two-phase relative permeability. SPE Reservoir Eng. 7:123–132. doi:10.2118/11015-PA

Hell, S.H., E.H.K. Stelzer, S. Lindek, and C. Cremer. 1994. Confocal microscopy with an increased detection aperture: Type-B 4Pi confocal microscopy. Opt. Lett. 19:222–224. doi:10.1364/OL.19.000222

Hematpour, H., M. Mardi, S. Edalatkhah, and R. Arabjamaloei. 2011. Experimental study of polymer flooding in low-viscosity oil using one-quarter five-spot glass micromodel. Pet. Sci. Technol. 29:1163–1175. doi:10.1080/10916460903514964

Hollman, R., and W.A. Little. 1981. Progress in the development of microminiature refrigerators using photolithographic fabrication techniques. In: J.E. Zimmerman et al., editors, Refrigeration for cryogenic sensors and electronic systems: Proceedings of a conference held at the National Bureau of Standards, Boulder, CO. 6–7 Oct. 1980. Natl. Bur. Standards Spec. Publ. 607. U.S. Gov. Print. Office, Washington, DC. p. 160–163.

Hornbrook, J.W., L.M. Castanier, and P.A. Pettit. 1991. Observation of foam/oil interactions in a new, high-resolution micromodel. Paper presented at: SPE Annual Technical Conference and Exhibition, Dallas, TX. 6–9 Oct. 1991. Paper 22631-MS.

Hug, T.S., D. Parrat, P.-A. Kunzi, U. Staufer, E. Verpoorte, and N.F. de Rooij. 2003. Fabrication of nanochannels with PDMS, silicon and glass walls and spontaneous filling by capillary forces. In: M.A. Northrup et al., editors, 7th International Conference on Miniaturized Chemical and Biochemical Analysis Systems, Squaw Valley, CA. 5–9 Oct. 2003. Vol. 1. Transducers Res. Foundation, San Diego. p. 29–32.

Huh, D., K.L. Mills, X. Zhu, M.A. Burns, M.A. Thouless, and S. Takayama. 2007. Tuneable elastomeric nanochannels for nanofluidic manipulation. Nat. Mater. 6:424–428. doi:10.1038/nmat1907

Hull, C. 1986. Apparatus for production of three-dimensional objects by stereolithography. U.S. Patent 4,575,330. Date issued: 11 Mar. 1986.

Iliescu, C., B. Chen, and J. Miao. 2008. On the wet etching of Pyrex glass. Sens. Actuators A 143:154–161. doi:10.1016/j.sna.2007.11.022

Jeong, S.W., and M.Y. Corapcioglu. 2003. A micromodel analysis of factors influencing NAPL removal by surfactant foam flooding. J. Contam. Hydrol. 60:77–96. doi:10.1016/S0169-7722(02)00054-2

Jeong, S.W., and M.Y. Corapcioglu. 2005. Force analysis and visualization of NAPL removal during surfactant-related floods in a porous medium. J. Hazard. Mater. 126:8–13. doi:10.1016/j.jhazmat.2005.06.015

Jeong, S.W., M.Y. Corapcioglu, and S.E. Roosevelt. 2000. Micromodel study of surfactant foam remediation of residual trichloroethylene. Environ. Sci. Technol. 34:3456–3461. doi:10.1021/es9910558

Johnston, W.G. 1962. Dislocation etch pits in non-metallic crystals with bibliography. In: J.E. Burke, editor, Progress in ceramic science. Vol. 2. Pergamon Press, New York. p. 1–75.

Kalaydjian, F. 1990. Origin and quantification of coupling between relative permeabilities for two-phase flows in porous media. Transp. Porous Media 5:215–229. doi:10.1007/BF00140013

Keane, R.D., and R.J. Andrian. 1992. Theory of cross-correlation analysis of PIV images. Appl. Sci. Res. 49:191–215. doi:10.1007/BF00384623

Keller, A.A., and M. Auset. 2007. A review of visualization techniques of biocolloid transport processes at the pore scale under saturated and unsaturated conditions. Adv. Water Resour. 30:1392–1407. doi:10.1016/j.advwatres.2006.05.013

Keller, A.A., M.J. Blunt, and P.V. Roberts. 1997. Micromodel observation of the role of oil layers in three-phase flow. Transp. Porous Media 26:277–297. doi:10.1023/A:1006589611884

Kim, E., Y. Xia, and G.M. Whitesides. 1996. Micromolding in capillaries: Applications in materials science. J. Am. Chem. Soc. 118:5722–5731. doi:10.1021/ja960151v

King, E., Y. Xia, X.-M. Zhao, and G.M. Whitesides. 1997. Solvent-assisted microcontact molding: A convenient method for fabricating three-dimensional structures on surfaces of polymers. Adv. Mater. 9:651–654. doi:10.1002/adma.19970090814

Kolari, K., V. Saarela, and S. Franssila. 2008. Deep plasma etching of glass for fluidic devices with different mask materials. J. Micromech. Microeng. 18:064010. doi:10.1088/0960-1317/18/6/064010

Lago, M., M. Huerta, and R. Gomes. 2002. Visualization study during depletion experiments of Venezuelan heavy oils using glass micromodels. J. Can. Pet. Technol. 41(1):02-01-03. doi:10.2118/02-01-03

Lanning, L.M., and R.M. Ford. 2002. Glass micromodel study of bacterial dispersion in spatially periodic porous networks. Biotechnol. Bioeng. 78:556–566. doi:10.1002/bit.10236

Lenormand, R. 1989a. Flow through porous media: Limits of fractal patterns. Proc. R. Soc. London Ser. A 423:159–168. doi:10.1098/rspa.1989.0048

Lenormand, R. 1989b. Application of fractal concepts in petroleum engineering. Physica D 38:230–234. doi:10.1016/0167-2789(89)90198-X

Lenormand, R., E. Touboul, and C. Zarcone. 1988. Numerical models and experiments on immiscible displacements in porous media. J. Fluid Mech. 189:165–187. doi:10.1017/S0022112088000953

Lenormand, R., and C. Zarcone. 1985a. Invasion percolation in an etched network: Measurement of a fractal dimension. Phys. Rev. Lett. 54:2226. doi:10.1103/PhysRevLett.54.2226

Lenormand, R., and C. Zarcone. 1985b. Two-phase flow experiments in a two-dimensional permeable medium. Physicochem. Hydrodyn. 6:497–506.

Lenormand, R., C. Zarcone, and A. Sarr. 1983. Mechanisms of the displacement of one fluid by another in a network of capillary ducts. J. Fluid Mech. 135:337–353. doi:10.1017/S0022112083003110

Lindek, S., C. Cremer, and E.H.K. Stelzer. 1996. Confocal theta fluorescence microscopy with annular apertures. Appl. Opt. 35:126–130. doi:10.1364/AO.35.000126

Lindken, R., M. Rossi, S. Grosse, and J. Westerweel. 2009. Micro-particle image velocimetry (microPIV): Recent developments, applications, and guidelines. Lab Chip 9:2551–2567. doi:10.1039/b906558j

Little, W.A. 1982. Microminiature refrigeration—small is better. Physica B+C 109–110:2001–2009. doi:10.1016/0378-4363(82)90564-2

Liu, Q. 2006. Interfacial phenomena in enhanced heavy oil recovery by alkaline flood. Ph.D. diss. Univ. of Regina, Regina, SK, Canada.

Liu, Y., D.D. Nolte, and L.J. Pyrak-Nolte. 2011. Hysteresis and interfacial energies in smooth-walled microfluidic channels. Water Resour. Res. 47:W01504. doi:10.1029/2010WR009541

Liu, Z., X. Yue, J. Hou, and L. Zhang. 2002. Comparison of displacement oil mechanism of polymer, ASP and foam of ASP in micro pores and dead ends of pores. Paper presented at: SPE Asia Pacific Oil and Gas Conference and Exhibition, Melbourne, Australia. 8–10 Oct. 2002. Paper 77876-MS.

Lovoll, G., M. Jankov, K.J. Maloy, R. Toussaint, J. Schmittbuhl, G. Schafer, and Y. Meheust. 2010. Influence of viscous fingering on dynamic saturation–pressure curves in porous media. Transp. Porous Media 86:335–354.

Lovoll, G., Y. Meheust, K.J. Maløy, E. Aker, and J. Schmittbuhl. 2005. Competition of gravity, capillary and viscous forces during drainage in a two-dimensional porous medium: A pore scale study. Energy 30:861–872. doi:10.1016/j.energy.2004.03.100

Mahers, E.G., and R.A. Dawe. 1985. Visualisation of microscopic displacement processes within porous media in EOR capillary pressure effects. In: 3rd European Meeting on Improved Oil Recovery, Rome. 16–18 Apr. 1985. Vol. 1. p. 40–58.

Markov, D.A., P.C. Samson, D.K. Schaffer, A. Dhummakupt, J.P. Wikswo, and L.M. Shor. 2010. Window on a microworld: Simple microfluidic systems for studying microbial transport in porous media. J. Vis. Exp. 39:e1741. doi:10.3791/1741

Marle, C.-M. 1981. From the pore scale to the macroscopic scale: Equations governing multiphase fluid flow through porous media. In: A. Verruijt and F.B.J. Barends, editors, Flow and Transport in Porous Media: Proceedings of Euromech 143, Delft, the Netherlands. 2–4 Sept. 1981. Taylor & Francis, Oxford, UK. p. 57–61.

Marle, C.M. 1982. On macroscopic equations governing multiphase flow with diffusion and chemical reactions in porous media. Int. J. Eng. Sci. 20:643–662. doi:10.1016/0020-7225(82)90118-5

Mattax, C.C., and J.R. Kyte. 1961. Ever see a water flood? Oil Gas J. 59:115–128.

McKellar, M., and N.C. Wardlaw. 1982. A method of making two-dimensional glass micromodels of pore systems. J. Can. Pet. Technol. 21(4):82-04-03. doi:10.2118/82-04-03

Meinhart, C.D., S.T. Wereley, and J.G. Santiago. 1999. PIV measurements of a microchannel flow. Exp. Fluids 27:414–419. doi:10.1007/s003480050366

Melchels, F.P.W., J. Feijen, and D.W. Grijpma. 2010. A review on stereolithography and its applications in biomedical engineering. Biomaterials 31:6121–6130. doi:10.1016/j.biomaterials.2010.04.050

Minsky, M. 1988. Memoir on inventing the confocal scanning microscope. Scanning 10:128–138.

Montemagno, C.D., and W.G. Gray. 1995. Photoluminescent volumetric imaging: A technique for the exploration of multiphase flow and transport in porous media. Geophys. Res. Lett. 22:425–428. doi:10.1029/94GL02697

Murakami, S.-I., T. Kuroda, and Z. Osawa. 1998. Dynamics of polymeric solid surfaces treated with oxygen plasma: Effect of aging media after plasma treatment. J. Colloid Interface Sci. 202:37–44. doi:10.1006/jcis.1997.5386

Naderi, K., and T. Babadagli. 2011. Visual analysis of immiscible displacement processes in porous media under ultrasound effect. Phys. Rev. E 83:056323. doi:10.1103/PhysRevE.83.056323

Nguyen, Q.P., M.H.G. Thissen, and P.L.J. Zitha. 2002. Effect of trapped foam on gas tracer diffusion in a visual microflow model. Paper presented at: SPE/DOE Improved Oil Recovery Symposium, Tulsa, OK. 13–17 April 2002. Paper 75208-MS. doi:10.2118/75208-MS

Nolte, D.D., and L.J. Pyrak-Nolte. 1991. Stratified continuum percolation: Scaling geometry of hierarchical cascades. Phys. Rev. A 44:6320–6333. doi:10.1103/PhysRevA.44.6320

Nolte, D.D., L.J. Pyrak-Nolte, and N.G.W. Cook. 1989. The fractal geometry of flow paths in natural fractures in rock and the approach to percolation. Pure Appl. Geophys. 131:111–138. doi:10.1007/BF00874483

Nourani, M., H. Panahi, D. Biria, R. Roosta Azad, M. Haghighi, and A. Mohebbi. 2007. Laboratory Studies of MEOR in Micromodel as a Fractured System. Paper presented at: Eastern Regional Meeting, Lexington, KY. 17–19 Oct. 2007. Paper 110988-MS. doi:10.2118/110988-MS

Nuss, W.F., and R.L. Whiting. 1947. Technique for reproducing rock pore space [in oil sands]. AAPG Bull. 31:2044–2049.

Ohara, J., K. Asami, Y. Takeuchi, and K. Sato. 2010. Development of RIE-lag reduction technique for Si deep etching using double protection layer method. IEEJ Trans. Electr. and Electron. Eng. 5:125–130. doi:10.1002/tee.20506

Okuda, R., Y. Sugii, and K. Okamoto. 2003. Velocity measurement of blood flow in a microtube using micro PIV system. In: Proceedings of the 4th Pacific Symposium on Flow Visualization and Image Processing, Chamonix, France. Univ. de Franche-Comte. 3–5 June 2003. Paper F4804.

Oren, P.E., J. Billiotte, and W.V. Pinczewski. 1992. Mobilization of waterflood residual oil by gas injection for water-wet conditions. SPE Form. Eval. 7:70–78. doi:10.2118/20185-PA

Park, S.-m., Y.S. Huh, H.G. Craighead, and D. Erickson. 2009. A method for nanofluidic device prototyping using elastomeric collapse. Proc. Natl. Acad. Sci. 106:15549–15554. doi:10.1073/pnas.0904004106

Paulsen, J.E., E. Oppen, and R. Bakke. 1998. Biofilm morphology in porous media: A study with microscopic and image techniques. Water Sci. Technol. 36:1–8. doi:10.1016/S0273-1223(97)00317-X

Perrin, C.L., K.S. Sorbie, and P.M.J. Tardy. 2005. Micro-PIV: A new technology for pore scale flow characterization in micromodels. Paper presented at: SPE Europec/EAGE Annual Conference, Madrid, Spain. 13–16 June 2005. Paper 94078-MS. doi:10.2118/94078-MS.

Pyrak-Nolte, L.J., N.G.W. Cook, and D.D. Nolte. 1988. Fluid percolation through single fractures. Geophys. Res. Lett. 15:1247–1250. doi:10.1029/GL015i011p01247

Pyrak-Nolte, L.J., D.D. Nolte, D. Chen, and N.J. Giordano. 2008. Relating capillary pressure to interfacial areas. Water Resour. Res. 44:W06408. doi:10.1029/2007WR006434

Quake, S.R., and A. Scherer. 2000. From micro- to nanofabrication with soft materials. Science 290:1536–1540. doi:10.1126/science.290.5496.1536

Rangel-German, E.R., and A.R. Kovscek. 2006. A micromodel investigation of two-phase matrix-fracture transfer mechanisms. Water Resour. Res. 42:W03401. doi:10.1029/2004WR003918

Rapoport, L.A., and W.J. Leas. 1951. Relative permeability to liquid in liquid–gas systems. J. Pet. Technol. 3:83–98.

Rogers, J.A., and R.G. Nuzzo. 2005. Recent progress in soft lithography. Mater. Today 8:50–56. doi:10.1016/S1369-7021(05)00702-9

Romano, M., M. Chabert, A. Cuenca, and H. Bodiguel. 2011. Strong influence of geometrical heterogeneity on drainage in porous media. Phys. Rev. E 84:065302(R). doi:10.1103/PhysRevE.84.065302

Romero, C., J.M. Alvarez, and A.J. Muller. 2002. Micromodel studies of polymer-enhanced foam flow through porous media. Paper presented at the SPE/DOE Improved Oil Recovery Symposium, Tulsa, OK. 13–17 Apr. 2002. Paper 75179-MS. doi:10.2118/75179-MS

Sagar, N.S., and L.M. Castanier. 1998. Pore-level visualization of oil–foam interactions in a silicon micromodel. In: Proceedings of the 11th SPE/DOE Improved Oil Recovery Symposium, Tulsa, OK. 19–22 Apr. 1998. Paper SPE 39512. Soc. Pet. Eng., Richardson, TX.

Sandnes, B., H.A. Knudsen, K.J. Måløy, and E.G. Flekkøy. 2007. Labyrinth patterns in confined granular–fluid systems. Phys. Rev. Lett. 99(3):038001. doi:10.1103/PhysRevLett.99.038001

Sato, Y., G. Irisawa, M. Ishizuka, K. Hishida, and M. Maeda. 2003. Visualization of convective mixing in microchannel by fluorescence imaging. Meas. Sci. Technol. 14:114–121. doi:10.1088/0957-0233/14/1/317

Sayegh, S.G., and D.B. Fisher. 2008. Enhanced oil recovery by CO2 flooding in homogeneous and heterogeneous 2D micromodels. Paper presented at: Canadian International Petroleum Conference, Calgary, AB. 17–19 June 2008. Paper 2008-005. doi:10.2118/2008-005.

Sbragaglia, M., R. Benzi, L. Biferale, S. Succi, K. Sugiyama, and F. Toschi. 2007. Generalized lattice Boltzmann method with multirange pseudopotential. Phys. Rev. E 75:026702. doi:10.1103/PhysRevE.75.026702

Semwogerere, D., and E.R. Weeks. 2005. Confocal microscopy. In: G. Wnek and G. Bowlin, editors, Encyclopedia of biomaterials and biomedical engineering. Taylor & Francis, New York.

Senn, T., J.P. Esquivel, M. Lörgen, N. Sabaté, and B. Löchel. 2010. Replica molding for multilevel micro-/nanostructure replication. J. Micromech. Microeng. 20:115012. doi:10.1088/0960-1317/20/11/115012

Sharma, J., S.B. Inwood, and A.R. Kovscek. 2011. Experiments and analysis of multiscale viscous fingering during forced imbibition. In: SPE Annual Technical Conference and Exhibition, Denver, CO. 30 Oct.–2 Nov. 2011. Paper 143946-MS. doi:10.2118/143946-MS

Shinohara, K., Y. Sugii, A. Aota, A. Hibara, M. Tokeshi, T. Kitamori, and K. Okamoto. 2004a. High-speed micro-PIV measurements of transient flow in microfluidic devices. Meas. Sci. Technol. 15:1965. doi:10.1088/0957-0233/15/10/003

Shinohara, K., Y. Sugii, K. Okamoto, H. Madarame, A. Hibara, M. Tokeshi, and T. Kitamori. 2004b. Measurement of pH field of chemically reacting flow in microfluidic devices by laser-induced fluorescence. Meas. Sci. Technol. 15:955–960. doi:10.1088/0957-0233/15/5/025

Shor, L.M., K.J. Rockne, L.Y. Young, G.L. Taghon, and D.S. Kosson. 2004. Combined effects of contaminant desorption and toxicity on risk from PAH contaminated sediments. Risk Anal. 24:1109–1120.

Sirivithayapakorn, S., and A. Keller. 2003. Transport of colloids in saturated porous media: A pore-scale observation of the size exclusion effect and colloid acceleration. Water Resour. Res. 39(4):1109. doi:10.1029/2002WR001583

Sohrabi, M., G.D. Henderson, D.H. Tehrani, and A. Danesh. 2001. Visualization of oil recovery by Water Alternating Gas (WAG) injection using high pressure micromodels: Oil-wet and mixed-wet systems. Paper presented at: SPE Annual Technical Conference and Exhibition, Dallas, TX. 1–4 Oct. 2000. Paper 63000-MS. doi:10.2118/63000-MS

Sohrabi, M., D. Tehrani, A. Danesh, and G.D. Henderson. 2004. Visualization of oil recovery by Water-Alternating-Gas injection using high-pressure micromodels. SPE J. 9(3):290–301.

Soll, W.E., M.A. Celia, and J.L. Wilson. 1993. Micromodel studies of three-fluid porous media systems: Pore-scale processes relating to capillary pressure–saturation relationships. Water Resour. Res. 29:2963–2974. doi:10.1029/93WR00524

Soudmand-asli, A., Sh. Ayatollahi, H. Mohabatkar, M. Zareie, and S.F. Shariatpanahi. 2007. The in situ microbial enhanced oil recovery in fractured porous media. J. Pet. Sci. Eng. 58:161–172. doi:10.1016/j.petrol.2006.12.004

Stewart, T.L., and H.S. Fogler. 2001. Biomass plug development and propagation in porous media. Biotechnol. Bioeng. 72:353–363. doi:10.1002/1097-0290(20010205)72:33.0.CO;2-U

Stewart, T.L., and H.S. Fogler. 2002. Pore-scale investigation of biomass plug development and propagation in porous media. Biotechnol. Bioeng. 77:577–588. doi:10.1002/bit.10044

Stöhr, M., K. Roth, and B. Jähne. 2003. Measurement of 3D pore-scale flow in index-matched porous media. Exp. Fluids 35:159–166. doi:10.1007/s00348-003-0641-x.

Stoner, D.L., S.M. Watson, R.D. Stedtfeld, P. Meakin, L.K. Griffel, T.L. Tyler, et al. 2005. Application of stereolithographic custom models for studying the impact of biofilms and mineral precipitation on fluid flow. Appl. Environ. Microbiol. 71:8721–8728. doi:10.1128/AEM.71.12.8721-8728.2005

Sugii, Y., S. Nishio, and K. Okamoto. 2002. In vivo PIV measurement of red blood cell velocity field in microvessels considering mesentery motion. Physiol. Meas. 23:403–416. doi:10.1088/0967-3334/23/2/315

Sugii, Y., and K. Okamoto. 2004. Quantitative visualization of micro-tube flow using micro-PIV. J. Vis. 7:9–16. doi:10.1007/BF03181480

Tallakstad, K.T., G. Lovoll, H.A. Knudsen, T. Ramstad, E.G. Flekkoy, and K.J. Maloy. 2009. Steady-state, simultaneous two-phase flow in porous media: An experimental study. Phys. Rev. E 80:036308. doi:10.1103/PhysRevE.80.036308

Theodoropoulou, M.A., V. Sygouni, V. Karoutsos, and C.D. Tsakiroglou. 2005. Relative permeability and capillary pressure functions of porous media as related to the displacement growth pattern. Int. J. Multiphase Flow 31:1155–1180. doi:10.1016/j.ijmultiphaseflow.2005.06.009

Thompson, L.F., C.G. Willson, and M.J. Bowden, editors. 1983. Introduction to microlithography. ACS Symp. Ser. 219. Am. Chem. Soc., Washington, DC.

Thompson, L.F., C.G. Willson, and M.J. Bowden, editors. 1994. Introduction to microlithography. 2nd ed. Am. Chem. Soc., Washington, DC.

Tóth, T., D. Horváth, and Á. Tóth. 2007. Density fingering in spatially modulated Hele–Shaw cells. J. Chem. Phys. 127:234506. doi:10.1063/1.2804426

Tretheway, D.C., and C.D. Meinhart. 2002. Apparent fluid slip at hydrophobic microchannel walls. Phys. Fluids 14:L9–L12. doi:10.1063/1.1432696

Tsakiroglou, C.D., and D.G. Avraam. 2002. Fabrication of a new class of porous media models for visualization studies of multiphase flow processes. J. Mater. Sci. 37:353. doi:10.1023/A:1013660514487

Tsakiroglou, C.D., D.G. Avraam, and A.C. Payatakes. 2007. Transient and steady-state relative permeabilities from two-phase flow experiments in planar pore networks. Adv. Water Resour. 30:1981–1992. doi:10.1016/j.advwatres.2007.04.002

Tsakiroglou, C.D., M.A. Theodoropoulou, and V. Karoutsos. 2003a. Nonequilibrium capillary pressure and relative permeability curves of porous media. AIChE J. 49:2472–2486. doi:10.1002/aic.690491004

Tsakiroglou, C.D., M. Theodoropoulou, V. Karoutsos, and D. Papanicolaou. 2005. Determination of the effective transport coefficients of pore networks from transient immiscible and miscible displacement experiments. Water Resour. Res. 41:W02014. doi:10.1029/2003WR002987

Tsakiroglou, C.D., M. Theodoropoulou, V. Karoutsos, D. Papanicolaou, and V. Sygouni. 2003b. Experimental study of the immiscible displacement of shear-thinning fluids in pore networks. J. Colloid Interface Sci. 267:217–232. doi:10.1016/S0021-9797(03)00635-0

Upadhyaya, A. 2001. Visualization of four-phase flow using micromodels. M.S. thesis. Stanford Univ., Stanford, CA. http://pangea.stanford.edu/ERE/pdf/pereports/MS/Upadhyaya01.pdf

van der Marck, S.C., and J. Glas. 1997. Pressure measurements during forced imbibition experiments in micro-models. Eur. J. Mech. B 16:681–692.

van Dijke, M.I.J., K.S. Sorbie, M. Sohrabi, D. Tehrani, and A. Danesh. 2002. Three-phase flow in WAG processes in mixed-wet porous media: Pore-scale network simulations and comparison with micromodel experiments. Paper presented at: SPE/DOE Improved Oil Recovery Symposium, Tulsa, OK. 13–17 April 2002. Paper 75192-MS. doi:10.2118/75192-MS

Vayenas, D.V., E. Michalopoulou, G.N. Constantinides, S. Pavlou, and A.C. Payatakes. 2002. Visualization experiments of biodegradation in porous media and calculation of the biodegradation rate. Adv. Water Resour. 25:203–219. doi:10.1016/S0309-1708(01)00023-9

Wan, J., T.K. Togunaga, C.F. Tsang, and G.S. Bodvarsson. 1996. Improved glass micromodel methods for studies of flow and transport in fractured porous media. Water Resour. Res. 32:1955–1964. doi:10.1029/96WR00755

Wan, J., and J.L. Wilson. 1994a. Visualization of the role of the gas–water interface on the fate of transport of colloids in porous media. Water Resour. Res. 30:11–23. doi:10.1029/93WR02403

Wan, J., and J.L. Wilson. 1994b. Colloid transport in unsaturated porous media. Water Resour. Res. 30:857–864. doi:10.1029/93WR03017

Wang, J., M. Dong, and K. Asghari. 2006. Effect of oil viscosity on heavy-oil/water relative permeability curves. Paper presented at: SPE/DOE Symposium on Improved Oil Recovery, Tulsa, OK. 22–26 Apr. 2006. Paper 99763-MS. doi:10.2118/99763-MS

Wang, W., L.M. Shor, E.J. LeBoeuf, J.P. Wikswo, and D.S. Kosson. 2005. Mobility of protozoa through narrow channels. Appl. Environ. Microbiol. 71:4628–4637. doi:10.1128/AEM.71.8.4628-4637.2005

Wang, W., L.M. Shor, E.J. LeBoeuf, J.P. Wikswo, G.L. Taghon, and D.S. Kosson. 2008. Protozoa migration in bent microfluidic channels. Appl. Environ. Microbiol. 74:1945–1949. doi:10.1128/AEM.01044-07

Wardlaw, N.C. 1980. The effects of pore structure on displacement efficiency in reservoir rocks and in glass micromodels. Paper presented at: SPE/DOE Enhanced Oil Recovery Symposium, Tulsa, OK. 20–23 Apr. 1980. Paper 8843-MS. doi:10.2118/8843-MS

Wegner, M.W., and J.M. Christie. 1983. Chemical etching of deformation substructures in quartz. Phys. Chem. Miner. 9:67–78. doi:10.1007/BF00308150

Weidman, T.W., and A.M. Joshi. 1993. New photodefinable glass etch masks for entirely dry photolithography: Plasma deposited organosilicon hydride polymers. Appl. Phys. Lett. 62:372–374. doi:10.1063/1.108960

Wereley, S.T., and C.D. Meinhart. 2005. Micron-resolution particle image velocimetry. In: K. Breuer, editor, Micro- and nano-scale diagnostic techniques. Springer-Verlag, New York.

Willingham, T.W., C.J. Werth, and A.J. Valocchi. 2008. Evaluation of the effects of porous media structure on mixing-controlled reactions using pore-scale modeling and micromodel experiments. Environ. Sci. Technol. 42:3185–3193. doi:10.1021/es7022835

Wyckoff, R.D., and H.G. Botset. 1936. The flow of gas–liquid mixtures through unconsolidated sands. J. Appl. Phys. 7:325–345. doi:10.1063/1.1745402

Xia, Y., and G.M. Whitesides. 1998. Soft lithography. Angew. Chem. Int. Ed. 37:550–575. doi:10.1002/(SICI)1521-3773(19980316)37:53.0.CO;2-G

Yeom, J., Y. Wu, J.C. Selby, and M.A. Shannona. 2005. Maximum achievable aspect ratio in deep reactive ion etching of silicon due to aspect ratio dependent transport and the microloading effect. J. Vac. Sci. Technol. B 23:2319–2329. doi:10.1116/1.2101678

Yeom, J., Y. Wu, and M.A. Shannon. 2003. Critical aspect ratio dependence in deep reactive ion etching of silicon. In: Proceedings of the 12th International Conference on Solid State Sensors, Actuators and Microsystems, Boston, MA. 9–12 June 2003. Vol. 2. IEEE, New York. p. 1631–1634.

Zang, W. 1998. Application of photo-luminescent volumetric imaging in multiphase dynamics in porous media. Ph.D. diss. Cornell Univ., Ithaca, NY.

Zekri, A.Y., and R.A. El-Mehaideb. 2002. Microbial and water flooding of fractured carbonate rocks: An experimental approach. Presented at: SPE/DOE Improved Oil Recovery Symposium, Tulsa, OK. 13–17 Apr. 2002. Paper 75217-MS. doi:10.2118/75217-MS

Zhang, C., K. Dehoff, N. Hess, M. Oostrom, T.W. Wietsma, A.J. Valocchi, et al. 2010. Pore-scale study of transverse mixing induced CaCO3 precipitation and permeability reduction in a model subsurface sedimentary system. Environ. Sci. Technol. 44:7833–7838. doi:10.1021/es1019788

Zhang, C., M. Oostrom, J.W. Grate, T.W. Wietsma, and M.G. Warner. 2011a. Liquid CO2 displacement of water in a dual-permeability pore network micromodel. Environ. Sci. Technol. 45:7581–7588. doi:10.1021/es201858r

Zhang, C., M. Oostrom, T.W. Wietsma, J.G. Grate, and M.G. Warner. 2011b. Influence of viscous and capillary forces on immiscible fluid displacement: Pore-scale experimental study in a water-wet micromodel demonstrating viscous and capillary fingering. Energy Fuels 25:3493–3505. doi:10.1021/ef101732k

Zhou, J., A.V. Ellis, and N.H. Voelcker. 2010. Editorial: Recent developments in PDMS surface modification for microfluidic devices. Electrophoresis 31:1. doi:10.1002/elps.200990124